EEG signatures of auditory activity correlate with simultaneously recorded fMRI responses in humans

Stephen D. Mayhew [a,*], Sharon G. Dirckx [a], Rami K. Niazy [a], Gian D. Iannetti [b], Richard G. Wise [c]

[a] Centre for Functional Magnetic Resonance Imaging of the Brain (FMRIB), Department of Clinical Neurology, John Radcliffe Hospital, Headington, Oxford, OX3 9DU, UK
[b] Department of Physiology, Anatomy and Genetics, University of Oxford, South Parks Road, Oxford, OX1 3QX, UK
[c] CUBRIC, School of Psychology, Cardiff University, Park Place, Cardiff, CF10 3AT, UK

ABSTRACT

We recorded auditory-evoked potentials (AEPs) during simultaneous, continuous fMRI and identified trial-to-trial correlations between the amplitude of electrophysiological responses, characterised in the time domain and the time–frequency domain, and the hemodynamic BOLD response. Cortical AEPs were recorded from 30 EEG channels within the 3 T MRI scanner with and without the collection of simultaneous BOLD fMRI. Focussing on the Cz (vertex) EEG response, single-trial AEP responses were measured from time-domain waveforms. Furthermore, a novel method was used to characterise the single-trial AEP response within three regions of interest in the time–frequency domain (TF-ROIs). The latency and amplitude values of the N1 and P2 AEP peaks during fMRI scanning were not significantly different from the Control session ($p > 0.16$). BOLD fMRI responses to the auditory stimulation were observed in bilateral secondary auditory cortices as well as in the right precentral and postcentral gyri, anterior cingulate cortex (ACC) and supplementary motor cortex (SMC). Significant single-trial correlations were observed with a voxel-wise analysis, between (1) the magnitude of the EEG TF-ROI1 (70–800 ms post-stimulus, 1–5 Hz) and the BOLD response in right primary (Heschl's gyrus) and secondary (STG, planum temporale) auditory cortex; and (2) the amplitude of the P2 peak and the BOLD response in left pre- and postcentral gyri, the ACC and SMC. No correlation was observed with single-trial N1 amplitude on a voxel-wise basis. An fMRI-ROI analysis of functionally-identified auditory responsive regions identified further single-trial correlations of BOLD and EEG responses. The TF amplitudes in TF-ROI1 and TF-ROI2 (20–400 ms post-stimulus, 5–15 Hz) were significantly correlated with the BOLD response in all bilateral auditory areas investigated (planum temporale, superior temporal gyrus and Heschl's gyrus). However the N1 and P2 peak amplitudes, occurring at similar latencies did not show a correlation in these regions. N1 and P2 peak amplitude did correlate with the BOLD response in bilateral precentral and postcentral gyri and the SMC. Additionally P2 and TF-ROI1 both correlated with the ACC. TF-ROI3 (400–900 ms post-stimulus, 4–10 Hz) correlations were only observed in the ACC and SMC. Across the group, the subject-mean N1 peak amplitude correlated with the BOLD response amplitude in the primary and secondary auditory cortices bilaterally, as well as the right precentral gyrus and SMC. We confirm that auditory-evoked EEG responses can be recorded during continuous and simultaneous fMRI. We have presented further evidence of an empirical single-trial coupling between the EEG and BOLD fMRI responses, and show that a time–frequency decomposition of EEG signals can yield additional BOLD fMRI correlates, predominantly in auditory cortices, beyond those found using the evoked response amplitude alone.

© 2009 Elsevier Inc. All rights reserved.

Introduction

EEG and fMRI are two neuroimaging techniques that are used to sample brain activity with complementary spatial and temporal resolution. Their simultaneous recording is especially desirable when variations in a subject's cognitive or physiological conditions mean that the brain activity under investigation cannot be

guaranteed as consistent between separate experimental sessions. It is increasingly used to study epilepsy where the EEG recording is used to indicate when epileptic discharges occurred during the fMRI acquisition (Salek-Haddadi et al., 2002; Gotman, 2008), and has been successfully applied to investigate spontaneous brain rhythms (Goldmann et al., 2002; Laufs et al., 2003; Moosmann et al., 2003), and sleep (Schabus et al., 2007). Simultaneous EEG–fMRI is especially important for investigating the possible causes of variability in the brain activity measured by EEG and fMRI during time-dependent effects such as habituation, attention or learning;

* Corresponding author. Fax: +44 1865 222717.
  E-mail address: smayhew@fmrib.ox.ac.uk (S.D. Mayhew).

and in drug studies, where between-session variability may be large (Iannetti and Wise, 2007).

EEG–fMRI allows the relationship between the trial-to-trial variations of electrophysiological and fMRI responses to be investigated with high temporal and spatial resolution (Debener et al., 2007b). The integration of EEG and fMRI data may reveal information not easily extracted from either technique alone. Assuming a linear neurovascular coupling relationship between the hemodynamic response, the local-field potential and the scalp EEG, the "integration by prediction" approach models the fMRI signal as a function of the EEG convolved with a canonical hemodynamic response function. This approach has proven successful for the treatment of single-trial evoked responses to establish correlations with the BOLD response using the auditory oddball P300 (Eichele et al., 2005; Benar et al., 2007) and the error-related negativity (Debener et al., 2005) as well as interictal epileptic activity (Salek-Haddadi et al., 2002) and resting alpha rhythms (Goldmann et al., 2002, Laufs et al., 2003).

Several authors have reported the successful recording of truly continuous and simultaneous EEG and fMRI responses to visual and somatosensory stimuli (Becker et al., 2005; Iannetti et al., 2005). However, simultaneous EEG–fMRI recordings of auditory stimulation are challenging due to the MR-acoustic environment, in addition to the necessary subtraction of the MRI artifacts from the EEG signal. Several previous attempts at recording auditory-evoked potentials (AEPs) during fMRI scanning have used an interleaved experimental paradigm with quiet periods for stimulus delivery (Liebenthal et al., 2003; Scarff et al., 2004a; Mulert et al., 2005; Debener et al., 2005, Eichele et al., 2005; Debener et al., 2007a) to avoid the potential confound of the MR-acoustic noise interfering with the auditory stimulus-evoked brain activity. Interleaving comes with the additional benefit of allowing recording of the EEG signal without contamination by MRI gradient artifacts. No direct comparisons between AEPs during fMRI to a Control measure without scanning were made, though Mulert et al. (2005), reported significant sound-level dependent increases in the amplitude of AEPs recorded outside the scanner that were not observed inside the fMRI scanner. These studies reported a close correspondence between ERP equivalent dipole source localisations and LORETA current source distributions compared with the extent of fMRI activation localised in the temporal cortex (Scarff et al., 2004a; Mulert et al., 2005). Interleaving EEG and fMRI acquisition has important practical and theoretical limitations, including inefficient sampling of the neural activity and the consequent hemodynamic response, and a reduction in the flexibility of the stimulus presentation paradigm.

The sound of the MRI scanner can induce a BOLD response in the cortical areas responsible for auditory processing, but is largely restricted to primary auditory cortex (Bandettini et al., 1998; Talavage et al., 1999; Hall et al., 2000; Scarff et al., 2004b). Several studies have shown that MR-related acoustic noise may actually interfere with the activation of the auditory cortex measured with fMRI during auditory stimulation (Cho et al., 1998) and phonetic discrimination (Shah et al., 1999). It has also been shown that auditory activation elicited by modulated tones in a high noise condition can result in a smaller number of activated voxels than a low noise condition (Elliot et al., 1998). The high-intensity noise generated by EPI imaging sequences can reduce auditory-related brain activity through psychophysiological masking and habituation effects (Edmister et al., 1999). It can also have an effect via the higher level cognitive load of discriminating between two different sounds presented at the same time (Belin et al., 1999). The response to the background scanner noise will lead to an elevated baseline activation level (Di Salle et al., 2003; Langers et al., 2005) and to a reduction in the dynamic range of the responses that experimental stimuli will induce (Edmister et al., 1999). Under the constant acoustic noise conditions of an fMRI study, a partial saturation of neuronal-evoked regional hemodynamics may occur which can reduce the BOLD signal amplitude in response to auditory

stimuli (Talavage and Edminster, 1998; Langers et al., 2005). The effect of acoustic MRI noise on the neuronal response to auditory stimulation itself has been less extensively investigated. Novitski et al. (2001) using recorded EPI noise at 54 dB, showed no significant difference in peak-to-peak amplitude of the N1 and P2 auditory-evoked potential (AEP) peaks evoked by 57 dB pure tones and chords.

As an alternative to the conventional measurement of event-related potential (ERP) peak amplitudes in the time-domain, time–frequency transforms provide a rich representation of ERP activity. In addition to the phase-locked activity that comprises the ERP wave-form, a stimulus can induce event-related oscillations that are time-locked but not phase-locked to the stimulus and represent frequency specific changes in the ongoing EEG. These specific changes may consist of either increases or decreases in power in given frequency bands relative to a pre-stimulus period and are known as event-related synchronisation (ERS) and event-related desynchronisation (ERD) respectively. Studies using analysis in the frequency domain have revealed that EEG oscillations and ERP peaks in different frequency ranges are functionally related to information processing and behaviour (Pantev et al., 1994; Pfurtscheller et al., 1997; Basar et al., 1999).

Signal processing techniques such as the wavelet transform facilitate the decomposition of the evoked potential into its constituent oscillatory and non-stationary signal components, and allow the analysis of event-related data in both the time and frequency domains. Consequently a time–frequency analysis is perceived as having the potential to reveal neurophysiological information not available to analyses restricted to the time domain (Demiralp et al., 1999; Mouraux et al., 2003; Mouraux and Iannetti, 2008). Recently, wavelet transform techniques have been used to assess non-phase-locked activity in auditory- (Demiralp et al., 1999; Makinen et al., 2004), visual- (Makeig et al., 2002) and laser-evoked potentials (Mouraux et al., 2003) as well as the unpredictable properties of epileptiform discharges (Adeli et al., 2003) and the fluctuations in the power of alpha and gamma frequency bands (Yordanova et al., 2002; Moosmann et al., 2003; Busch et al., 2004).

In the present study we characterise and compare single-trial measures of AEP response amplitude in both the time- and the time–frequency domains as electrophysiological predictors of the BOLD response. We hypothesise that trial-to-trial variability in the AEP response is reflected in the BOLD time-series. We also investigate whether intersubject variability in the AEP amplitude is reflected in the BOLD signal.

Our investigation further evaluates whether robust and repeatable AEPs can be recorded during truly continuous, simultaneously acquired BOLD fMRI at 3 T. By comparing AEPs recorded during fMRI to recordings inside the scanner but without fMRI, we aim to assess whether AEP data quality is degraded by the combined effects of acoustic scanner noise and MRI gradient artifact removal.

Methods

Experimental paradigm

12 healthy volunteers (3 females, age range 23–32 years) participated in this study. All subjects gave their informed consent and the local ethics committee approved the procedures. For each subject, AEPs were recorded in two sessions conducted on the same day. In the 'fMRI session', AEPs were recorded during continuous fMRI at 3 T. In the 'Control session', AEPs were recorded within the MRI scanner but without fMRI acquisition. The order of the sessions was balanced across subjects.

The auditory stimulation consisted of a 100 ms-long, 1 kHz electronic pure tone delivered via pneumatic tubing to passive ER-30 earphones (www.etymotic.com) inserted inside the acoustic canal. These earphones were mounted inside ear defenders which reduced

MRI acoustic noise by 30 dB. Auditory stimuli were presented in a block design, with 30 s of stimulation (12 stimuli at 0.4 Hz) followed by 30 s of silence. The sound pressure level of the stimulus presentation was 65 dB and was kept constant across subjects. Subjects were asked to remain alert with their eyes open, to relax their muscles and attend to the stimulus.

EEG recording

The EEG recording parameters were identical during both fMRI and Control sessions. EEG was recorded with 30 Ag/AgCl electrodes placed on the head using an MRI compatible cap (Easycap, www.easycap.de), according to the 10–20 system, using the nose as extracephalic reference. Current limiting safety resistors (5 kΩ) were applied on each electrode lead close to the electrode itself, to limit the induced current and minimise lead loops. Total electrode impedance was kept below 15 kΩ. In order to identify trials contaminated by eyeblinks, electroculographic (EOG) signals were recorded using surface electrodes, one placed over the mid-lower eyelid and the other 1 cm lateral to the lateral corner of the orbit. In order to subtract the ballisto-cardiographic (BCG) artifact, the electrocardiogram (ECG) was also recorded from bipolar electrodes attached to the subject's chest during both sessions. ECG and EOG channels had 100 kΩ current-limiting safety resistors. All cables were twisted and harnessed in a plastic tube. EEG data was digitised with an MR-compatible, 22-bit, 32-channel amplifier (SD-MRI, Micromed, Italy): bandwidth 0.15–600 Hz, sampling rate 2048 Hz, input dynamic range ±26.5 mV.

fMRI recording

BOLD fMRI scanning was performed continuously on Varian INOVA 3 T MRI system. A 4-channel, head-only receive coil was used with a head-only birdcage transmit coil. A continuous, whole-brain T2* weighted, gradient-echo EPI sequence was used for the functional scans (TR = 3 s, TE = 30 ms, 43 contiguous 3-mm-thick axial slices (voxel size $3 \times 3 \times 3$ mm), image matrix 64×64, flip angle 90°) over 184 volumes, corresponding to a total scan time of 9 min. Furthermore for each subject, a T1-weighted, high-resolution structural image (70 contiguous 3-mm-thick axial slices, in plane field of view 256×192 mm, matrix 256×192) was collected for anatomical overlay of brain activation and registration.

EEG data pre-processing

All EEG data were imported and analysed using EEGLAB (www.sccn.ucsd.edu/eeglab) (Delorme and Makeig, 2004). MRI gradient artifacts in the fMRI session and the BCG artifacts in both fMRI and Control sessions were removed using the FASTR and OBS algorithms respectively (Niazy et al., 2005).

FASTR works by subtracting an averaged gradient artifact template from each EEG channel, that is constructed using windowed averaging of synchronised fMRI slice triggers. An additional step estimates and removes the residual artifact using basis functions derived from a principal components analysis (PCA) of the artifact segments of each channel. To remove the BCG artifact from the data an optimal basis set (OBS) is constructed using a PCA decomposition of the matrix of BCG events detected by an adaptive thresholding algorithm. The OBS is formed from the 3 principle components that explain the most significant variance in the BCG signal, and is then subtracted from the data (Niazy et al., 2005).

Analysis of the EEG data focussed on the vertex (Cz) channel as this shows the strongest response and because is one of the most commonly used sites for reporting the late AEPs allowing us to investigate common variability in the BOLD signal and a robust electrophysiological response.

Continuous EEG data (from Cz-ref) was downsampled to 256 Hz and band-pass filtered from 0.5–40 Hz. EEG epochs containing the auditory stimuli were extracted using a window of 2 s (from 1000 ms pre-stimulus to 1000 ms post-stimulus). For each epoch, a baseline correction for the pre-stimulus data was performed. EEG recordings were manually inspected and trials contaminated with gross movements were rejected. In a second stage of the analysis, an ICA decomposition using the infomax algorithm (Bell and Sejnowski, 1995) was performed. In each subject, a single component containing the transient eye-blink artifacts was removed from both the fMRI and Control session datasets. This component was identified from its ERP image which possessed a distinctive pattern of transient deviations with large amplitude occurring at unpredictable latency within AEP epochs, and also a scalp electric-field map with an obvious frontal weighting. Both of these are quite distinct from ERP images and scalp maps belonging to signals of neurophysiological origin. Furthermore, components that significantly correlated with the recorded ECG signal were rejected as residual BCG artifacts, in accordance with a recently published processing strategy (Debener et al., 2007a). The grand-mean AEP average waveform across subjects was also calculated for comparison between fMRI and the Control sessions. Finally, the signal-to-noise ratio of each subject's mean AEP, from both Control and fMRI sessions, was calculated by dividing the amplitude of the N1 peak by the standard deviation of the −500 ms to 0 ms pre-stimulus data (Debener et al., 2007a,b).

Evaluation of the effect of MRI-artifact removal on AEP amplitudes

One aim of the study is to compare AEPs recorded during fMRI to AEPs recorded without fMRI scanning. In this context, it is important to clarify whether any observed differences could be due to altered neuronal activity or due to the implemented MR-artifact correction. Recent studies have demonstrated that, in some cases, MRI-artifact correction causes degradation of the physiological EEG (Grouiller et al., 2007; Ritter et al., 2007). Here we have used real EEG data to simulate new datasets for each of 3 representative subjects with which to investigate the effect of the FASTR MR-artifact correction upon the amplitude of evoked potentials.

The block experimental design used in this study contained 30 s periods of auditory stimulation separated by 30 s periods where no auditory stimulus was delivered. These 'off' periods therefore contained no stimulus and the underlying EEG is a good approximation to resting EEG. This was used as the background EEG onto which a template ERP was superimposed. The template ERP was created from the averaged AEP epochs recorded during the Control session (epoched from −1000 ms pre-stimulus to +1000 ms post-stimulus). These control AEPs had been pre-processed as previously described, filtered 0.5–45 Hz, downsampled to 512 Hz and then BCG artifacts removed using the OBS method. We added 11 template ERPs into each of the eight 'off' blocks in each recording. This created 88 simulated AEPs in total for each dataset, a similar number to the original recordings. An inter-stimulus interval of 2.5 s was used, to match that of the original AEPs.

Identical pre-processing was performed upon both the simulated ERP dataset and a comparison dataset of the original 'off' periods between the auditory stimulation (with no ERPs added). All the following parameters used were identical to those in the processing of the original AEP data. FASTR (averaging window length = 30, up-sampling frequency 20 kHz), filtered 0.5–45 Hz, downsampled to 512 Hz and then BCG artifacts removed using the OBS method. Both datasets were epoched to the same intervals (−1000 ms pre-stimulus to +1000 ms post-stimulus) and baseline corrected for the pre-stimulus data. Both the simulated and original corrected datasets were visually inspected and trials containing gross movements were rejected from both datasets. The number of trials remaining was 86, 84 and 87 for Subjects 1, 2 and 3 respectively. Finally, across trial

averaging was performed in order to display results. The recovered Template ERP was computed by subtracting the corrected original data (without AEPs added) from the corrected simulated data (with AEPs added before correction). The recovered Template ERP allows visual assessment of the data quality, by comparison with the Template ERP that was added to the data. Any FASTR-induced significant degradation of the AEP data would result in a difference in the amplitudes of these two waveforms.

Dipole source analysis

Dipole source localisation of our main AEP responses was also performed. We focussed on localising sources of the group average waveforms of the fMRI and Control sessions across 30 scalp channels.

The data interval for source analysis was determined by computing the mean global field power (MGFP). The MGFP is a measure of the instantaneous variance across all electrodes for each time point in the mean AEP. MGFP therefore provides a robust measure for identifying maximal time points of cortical activity, that encompasses the data at all recorded electrodes. The group mean N1 peak latency was identified from the MGFP for both fMRI and Control sessions. The data interval for source analysis was centered upon the N1 peak latency, encompassing a window ± 20 ms (Scarff et al., 2004a).

The averaged AEPs were further filtered between 1–20 Hz and equivalent current dipole modeling was performed using Curry 6 (Compumedics Neuroscan, Charlotte USA). A standard spherical head model was used with 4-shells to represent the brain, dura, skull and skin layers with default radii and conductivity parameters. To estimate source activity, a two-dipole model was used to estimate symmetrical (with respect to the midline) sources in both hemispheres (minimally 25 mm apart). The source location, orientation, and strength parameters were iteratively adjusted until the residual variance (difference between the recorded versus modeled activity) was minimised. Source solutions for Control and fMRI sessions were then overlaid on the MNI standard brain.

Single-trial EEG measurements

Time-domain amplitudes

After pre-processing and artifact removal, the amplitude of the N1 and P2 peaks for each single-trial AEP were measured using a multiple-linear regression method described fully in Mayhew et al., 2006. In summary of this method, single-trial N1 and P2 amplitudes from AEP epochs recorded during both Control and fMRI sessions were measured independently for each subject by constructing a basis set of four regressors derived from the time-domain average waveforms of the N1 and P2 evoked-potential peaks and their respective temporal derivatives. This average basis set is then regressed against each single-trial AEP epoch in a procedure that is analogous to the GLM commonly used in fMRI analysis. Single-trial AEP amplitude and latency measurements are obtained from the linear sum of the basis-set regressors multiplied by the corresponding regression coefficients. For each subject, the mean single-trial value of N1 and P2 peak amplitude and N1 and P2 peak latency were calculated. These measurements were then used to test for any significant differences in N1 or P2 amplitude or latency between the fMRI and Control sessions across the group (two-tailed paired t-test).

Time–frequency domain amplitudes

The time–frequency matrix (TFM) of each single-trial AEP was calculated with the LetsWave software package (http://amouraux. webnode.com/letswave/) using the continuous Morlet wavelet transform: frequency range (F) 1–30 Hz in increments of 0.5 Hz; time range (T) 500 ms pre-stimulus to 1000 ms post-stimulus with a resolution of 0.8 ms. The post-stimulus TFM was baseline corrected using the pre-stimulus data. The result of the wavelet transform is an expression of both phase-locked and non-phase-locked oscillation amplitudes, hereafter referred to as TF amplitude.

TFMs create a significant increase in information from the one-dimensional time domain. Consequently, reducing this information into a set of parameters characterising meaningful activity is more complex than in one-dimension alone. Recent studies have shown
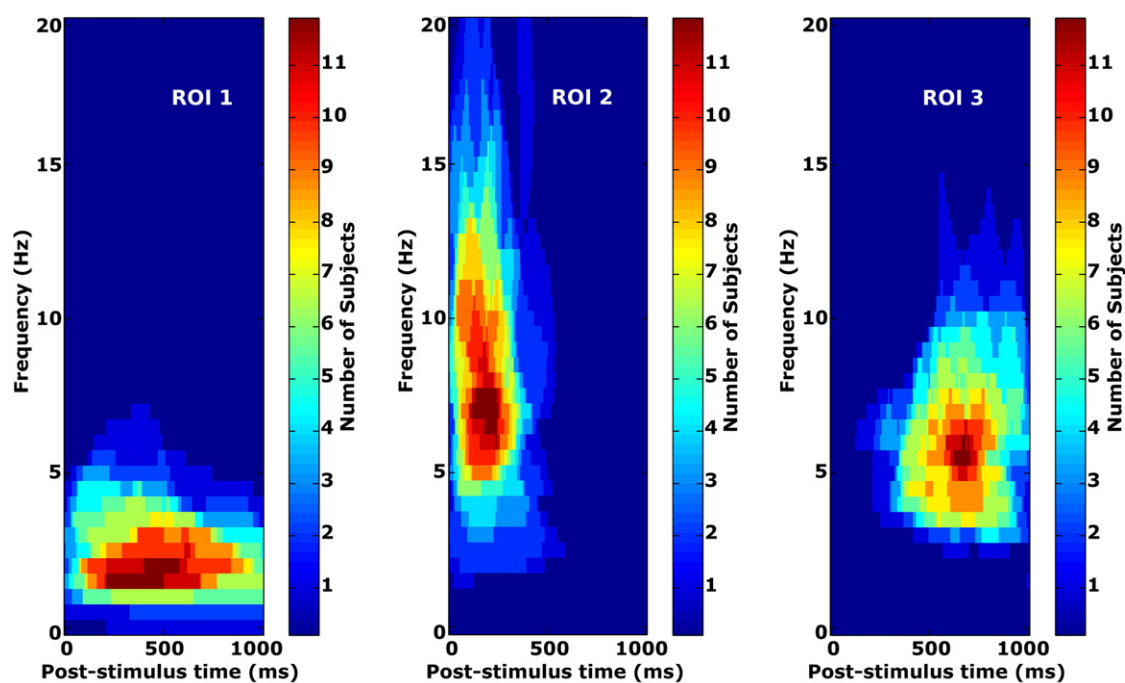

Fig. 1. Group conjunction of TF-ROIs. The consistency of the definition of TF-ROI1, TF-ROI2 and TF-ROI3 across fMRI session data for all subjects is shown ($N = 12$). The colour scale reflects the number of subjects in which that pixel of the time–frequency plane was present in each respective TF-ROI. Within each TF-ROI, the mean TF amplitude for each single-trial AEP was calculated, providing three characterisations of the AEP response in the time–frequency domain.

principal components analysis to be a suitable mathematical tool for extracting joint time–frequency components from the TFMs of single-trial evoked potentials (Bernat et al., 2005, 2007). It allows the characterisation of meaningful neuroelectric events that can span arbitrary ranges both in time and frequency. The PCA procedure used in this study followed that outlined in Bernat et al., 2005 and is summarised here.

PCA decomposition was performed independently for each individual subject. Each single-trial TFM (F×T) was re-arranged into a vector (1×FT) and all vectors were stacked to form a single data matrix (dimensions: trials×FT). This manipulation recasts the data with trials in rows and time points of activity in columns. PCA decomposition of the covariance matrix was performed with varimax rotation of components. The resultant principal component (PC) vectors were then re-arranged into matrices by applying the reverse data manipulation, creating PC matrices that possess the same dimensions (F×T) as the original single-trial TFMs. Principal component matrices were then assigned to form TF-ROIs based on classifying the temporal range, frequency range, and percentage of variance in the data explained by each PC. Firstly, only the four PCs that explained the maximum variance in the data were considered. Across subjects these PCs were then arranged into groups with similar time–frequency profiles. The selection of TF-ROIs was based on a-priori knowledge of the regions of interest within the time–frequency plane according to the findings of previous work. It has been shown that many modalities of evoked potentials possess three consistent areas of activity in the time–frequency plane (Mouraux et al., 2003; Makinen et al., 2004). The analysis in this study was interested in characterising these regions in AEPs using a data-driven approach.

For nine of the twelve subjects, the three PCs that explained the largest amount of variance were the ones that formed the TF-ROIs of interest. However, within these three PCs there was no reliable ordering, so in this work we did not implement TF-ROI selection based solely on the amount of variance explained. In all subjects, PCA revealed two regions of event-related synchronisation (ERS): TF-ROI1, mean latency range 73–856 ms post-stimulus, mean frequency range 1.1–4.6 Hz; TF-ROI2, mean latency range 24–442 ms, mean frequency range 4.9–14.3 Hz. A third region of event-related desynchronisation (ERD) was observed, TF-ROI3, mean latency range 451–912 ms, mean frequency range 3.8–10.3 Hz. Similar transient responses in the time–frequency plane have been previously reported (Krause, 1999; Cacace and McFarland, 2003; Makinen et al., 2004). A conjunction plot showing the consistency of these three TF-ROIs across the group of subjects is shown in Fig. 1.

For each subject, the selected principal components were thresholded so as to null the low amplitude signals-of-no-interest that are treated as noise in the TFM. A cut-off was chosen whereby only activity with amplitude larger than two standard deviations above the mean was preserved. These thresholded PCs formed the subject-specific TF-ROIs which were then multiplied with the single-trial AEP TFMs to yield the mean TF amplitude within each of the subject-specific TF-ROIs. This extracted three summary TF-amplitude parameters for each trial. Finally, the group mean AEP TFM was calculated for the fMRI and Control conditions (Fig. 2).

In addition, the group mean scalp distribution of TF amplitude for each of the three TF-ROIs from the AEP responses recorded during fMRI scanning was calculated. Group average TF-ROI1, TF-ROI2 and TF-ROI3 were defined from the mean of the time and frequency dimensions of the individual subject TF-ROIs. The three group TF-
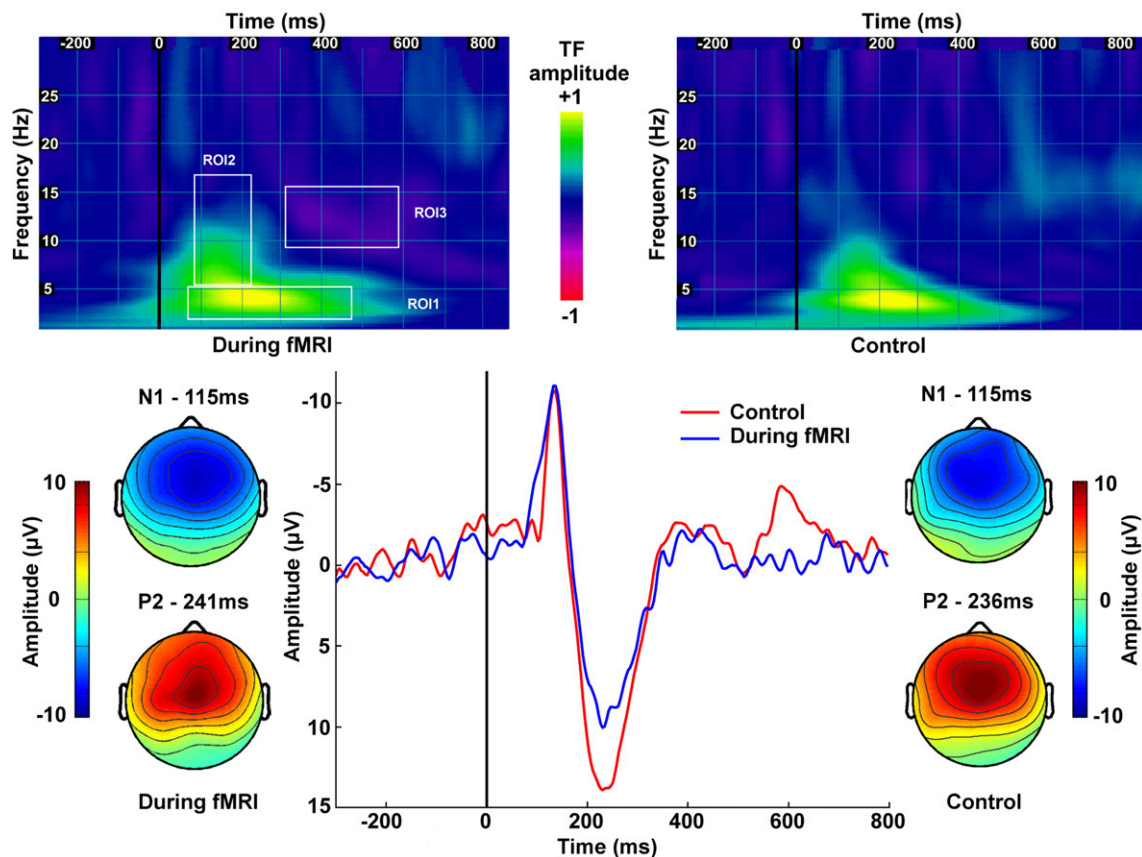

Fig. 2. Summary of AEP recordings during fMRI and Control sessions. Group mean AEP waveforms (Cz-ref) recorded during: fMRI session (blue); Control session (inside scanner, no fMRI, red). Scalp maps of the electric-field distribution for the N1 and P2 peaks are also shown for fMRI session (left) and Control session (right) respectively. Upper panel: Group mean wavelet transform of single-trial AEPs acquired during fMRI session (left) and Control session (right). White boxes illustrate the location of TF-ROI1, TF-ROI2 and TF-ROI3 used for extraction of single-trial time–frequency amplitudes.

ROIs were then multiplied with the group mean AEP TFM to yield the group mean TF amplitude within each of the group TF-ROIs, which was used to plot the scalp maps. The resultant maps represent the distribution of TF amplitude at the centre of each TF-ROIs latency and frequency range (Supplementary Fig. 4).

fMRI data processing

All fMRI analyses were carried out using FSL 4.0 (FMRIB's Software Library, www.fmrib.ox.ac.uk/fsl). Prior to statistical analysis the following pre-processing was applied: automated brain extraction using BET (Smith, 2002) and motion correction using MCFLIRT (Jenkinson et al., 2002) was performed before spatial smoothing using a Gaussian kernel (5 mm FWHM), and high-pass temporal filtering (Gaussian-weighted least-squares straight line fitting, filter cut-off of 60 s). Single-subject time-series statistical analysis was carried out using FILM with local autocorrelation correction (Woolrich et al., 2001). Z-statistic images were thresholded using clusters determined by $Z>2.0$ and a (corrected) cluster significance threshold of $p<0.05$. Registration to high-resolution structural and standard images was carried out using FLIRT (Jenkinson and Smith, 2001).

Single-trial single-subject EEG–fMRI correlations

Single-trial measurements of N1, P2 amplitude and the TF amplitude of TF-ROI1, TF-ROI2 and TF-ROI3 were used to form regressors to investigate whether the voxel-wise amplitude of the BOLD signal correlated with the amplitude of the AEP responses. Six regressors were used in each subject-level analysis, the first represented the mean amplitude of the response (a box-car function); the other five regressors represented the trial-to-trial variability in the respective EEG response amplitude (single-trial measures demeaned).

Including all EEG measures as separate regressors in the same fMRI GLM will enable us to determine which fMRI correlations are most significantly associated with the different measures of the AEP response. Positive contrasts were then set on all six regressors to show the mean auditory response (contrast vector [1, 0, 0, 0, 0, 0]) and also show in what brain areas the fMRI signal correlates with each individual AEP measure (contrast vectors, N1 [0, 1, 0, 0, 0, 0], P2 [0, 0, 1, 0, 0, 0], TF-ROI1 [0, 0, 0, 1, 0, 0], TF-ROI2 [0, 0, 0, 0, 1, 0], TF-ROI3 [0, 0, 0, 0, 0, 1]). In addition, two contrasts were calculated to directly compare the significance of N1 and P2-BOLD correlations to TF-ROI1 and 2-BOLD correlations: N1 and P2>TF-ROI1 and TF-ROI2 (contrast vector [0, 1, 1, −1, −1, 0]); TF-ROI1 and TF-ROI2>N1 and P2 (contrast vector [0, −1, −1, 1, 1, 0]).

These two contrasts provide a statistical measure of where in the brain the variability in the fMRI signal associated with N1 and P2 is greater than the fMRI variability associated with TF-ROI1 and 2 amplitudes, and vice versa. This is important as it provides information about which AEP response measure is best correlated with the fMRI signal in a given brain area. One of the goals of this paper was to compare the fMRI correlates of AEP time-domain amplitude with time–frequency domain amplitudes. We chose to compare TF-ROIs 1 and 2 with N1 and P2 amplitudes as they span the same latency ranges. Restricting the comparison to the same latencies for both measures provides a fairer comparison for whether the TF-ROI measures explain a greater degree of variance in the fMRI signal than the more conventional N1 and P2 amplitude measures, while maintaining the possibility that they represent similar underlying electrophysiological phenomena.

A mixed-effects group analysis ($Z>2.0$, $p<0.05$ cluster-corrected) using FLAME 1 and 2 (Woolrich et al., 2004) was performed and Z-statistic maps for mean BOLD activation, and group average single-trial BOLD variability in response to the auditory stimulus were computed.

EEG–BOLD correlations were also investigated using an fMRI region of interest (ROI) analysis of those regions significantly active in response to the main effect of auditory stimulation across the group. The thresholded, cluster-corrected statistical map of the group activation to the mean stimulus effect was used to define eight functional ROIs. The bilateral clusters of auditory activation in primary and secondary auditory areas were used as a broad definition of the active region of auditory cortex (MAS). Specific functional ROIs were also defined by masking the mean auditory response with bilateral anatomical masks of: superior temporal gyrus, Heschl's gyrus, planum temporale, precentral gyrus, post-central gyrus, supplementary motor cortex and anterior cingulate cortex. For each subject, these functional ROIs were used to extract the mean regional percentage BOLD signal change associated with each single-trial measure of the AEP response. The purpose of this additional analysis was to investigate which of the brain areas that were measured as active in response to the mean effect of the auditory stimulus, also possessed activity that correlated with the trial-by-trial variation in AEP response amplitude. Additional functional ROIs were defined in the right putamen and thalamus as we thought it interesting to investigate whether fMRI responses in subcortical areas correlated with scalp EEG responses. All anatomical masks were obtained from the Harvard cortical masks (in the standard space of the Montreal Neurological Institute) in the FMRIB software library (FSL).

Group-level EEG–fMRI correlations

The correlation across the group between the mean BOLD response and mean amplitude of the N1 and P2 peaks for each subject was also investigated. In this new group analysis it was the between-subject variation in the mean stimulus effect that was of interest, and not the single-trial variability. Statistical analysis was only performed on the first regression coefficient carried up from the single-subject level. Two separate group-level GLMs were created, each using two regressors. The first regressor represented the group mean single-trial amplitude of the N1 or P2 peak respectively. The second regressor was formed from the between-subject variability in the mean single-trial N1 or P2 peak amplitudes respectively. Mixed-effects group analyses were performed ($Z>2.0$, $p<0.05$ cluster-corrected) and Z-statistic maps for mean BOLD activation, and group-level BOLD variability in response to the auditory stimulus were computed for the N1 and P2 peaks. An fMRI-ROI analysis was again used to extract the mean regional percentage BOLD signal change from the eight areas described above. This was then used to investigate correlations between the amplitude of subjects' BOLD response and the amplitude of the mean N1 and P2 peaks.

Results

Auditory EEG responses

All subjects reported after the experiment that they had heard the stimuli without difficulties. Auditory stimulation evoked clear and reproducible AEPs time-locked to the stimulus. Fig. 2 shows the group mean AEP waveforms, scalp maps of N1 and P2 peaks and group mean AEP TFM calculated from single-trial Cz-ref data recorded during both the fMRI and the Control sessions. The earliest identifiable response observed was the negative peak (N1). For N1, the amplitude and latency from the ERP grand average were 11.2 µV and 115 ms respectively, during the fMRI session and 11.2 µV and 115 ms during the Control session. For P2, the amplitude and latency from the ERP grand average were 9.9 µV and 236 ms respectively, during the fMRI session and 11.7 µV and 241 ms during the Control session. The main negative (N1) and positive (P2) peaks have a maximum scalp electric field at the vertex for both fMRI and Control sessions.
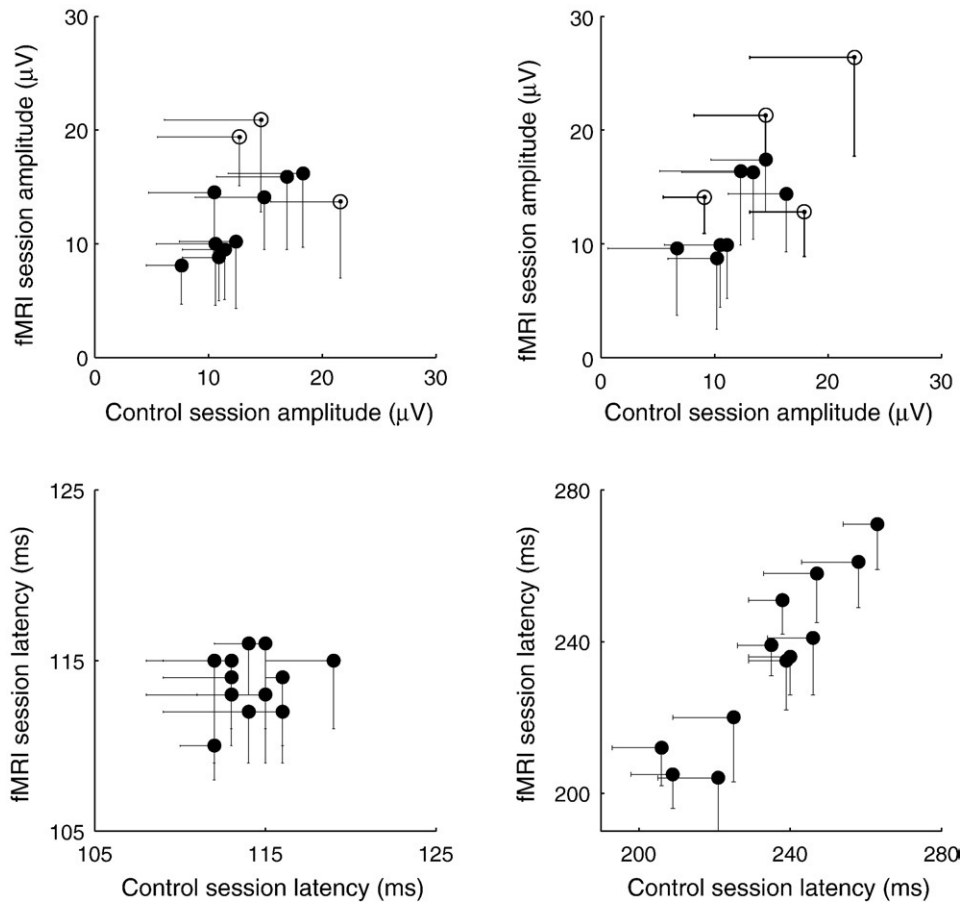
Fig. 3. Comparison of N1 and P2 peak amplitude and latency between fMRI and Control sessions. Each data point represents the mean single-trial amplitude (upper row) or latency (lower row) of the N1 and P2 peaks measured from all trials recorded from each subject during fMRI and during Control sessions (error bars represent standard deviation). Open circles represent individual subject's amplitudes that were significantly different between fMRI and Control sessions ($p < 0.05$, two-tailed t-test).

The scalp distributions of TF amplitude obtained from group TF-ROI1, 2 and 3 (Supplementary Fig. 4) are very similar to those of the N1 and P2 peaks of the time-domain AEP waveforms, showing a maximum scalp TF amplitude at the vertex electrode. Although no information is provided about the exact cortical origin of these TF-ROI responses, these scalp maps provide no reason to expect their sources to be different to those of the time-domain AEP peaks.

The grand-mean averaged AEP (Fig. 2) shows evidence of a later peak in the Control session, occurring approximately 600 ms post-stimulus, that is not observed in the average from the fMRI session. Examination of the individual subject average waveforms revealed that seven subjects exhibited this N600 peak, in addition to the N1 and P2 peaks, during the Control session, compared to four subjects during the fMRI session.

The results of the evaluation of the MR-artifact correction can be viewed in Supplementary Fig. 2. For all three subjects, the template and the recovered template ERPs are extremely similar, both in N1 and P2 peak amplitudes and in general appearance of the waveforms. The N1 amplitude of the recovered template ERP is approximately 1 μV less than the template ERP in Subjects 1 and 2. The P2 amplitude of the recovered template ERP is approximately 2 μV less than the template ERP in Subject 2. No differences were found between the amplitude of the recovered and template ERPs of Subject 3.

Fig. 3 displays the averaged single-trial amplitude and latencies of the N1 and P2 peaks, obtained by automated measurement, for all subjects. The respective group mean amplitude and latency measurements are displayed in Table 1. By comparing subjects' mean single-trial values, no significant difference was measured between the fMRI and Control sessions in either the amplitude or the latency of the N1

and P2 peaks across the group (N1: amplitude $p > 0.5$, latency $p > 0.5$, P2: amplitude $p > 0.1$, latency $p > 0.5$). Fig. 3 and Table 1 suggest a trend towards a larger P2 peak in the Control session, although this did not reach statistical significance ($p > 0.16$). The mean N1 amplitudes in two individual subjects were measured as significantly smaller during the fMRI session compared to the Control session, and three subjects showed significantly smaller P2 amplitude during fMRI. In addition, one subject had mean N1 and P2 amplitudes that were significantly larger during the fMRI session than during the Control session (all $p < 0.05$, two-tailed t-test). These subjects are denoted by the open circles in Fig. 3. The AEP SNR, according to a measure used in a recent study (Debener et al., 2007a,b), was very similar between the fMRI and Control sessions. fMRI session, (mean ± standard deviation) SNR 7.4 ± 2.0; Control session, SNR 7.6 ± 2.2. No significant difference was found between the SNR of the two sessions ($p > 0.6$, paired t-test, $N = 12$).

The intersubject variability in our measured AEP amplitudes was relatively high, therefore our statistical power to detect an observed change in N1 or P2 amplitude across the group is relatively low (for P2

Table 1
Group average single-trial AEP measurements.

	Amplitude (μV)		Latency (ms)	
	N1	P2	N1	P2
fMRI	13.4 ± 3.9	13.2 ± 4.3	113 ± 3	236 ± 20
Control	13.4 ± 4.1	14.8 ± 5.3	114 ± 2	236 ± 17

Group mean single-trial amplitude and latency of AEP N1 and P2 peaks for all trials acquired during fMRI and during Control sessions (± standard deviation).
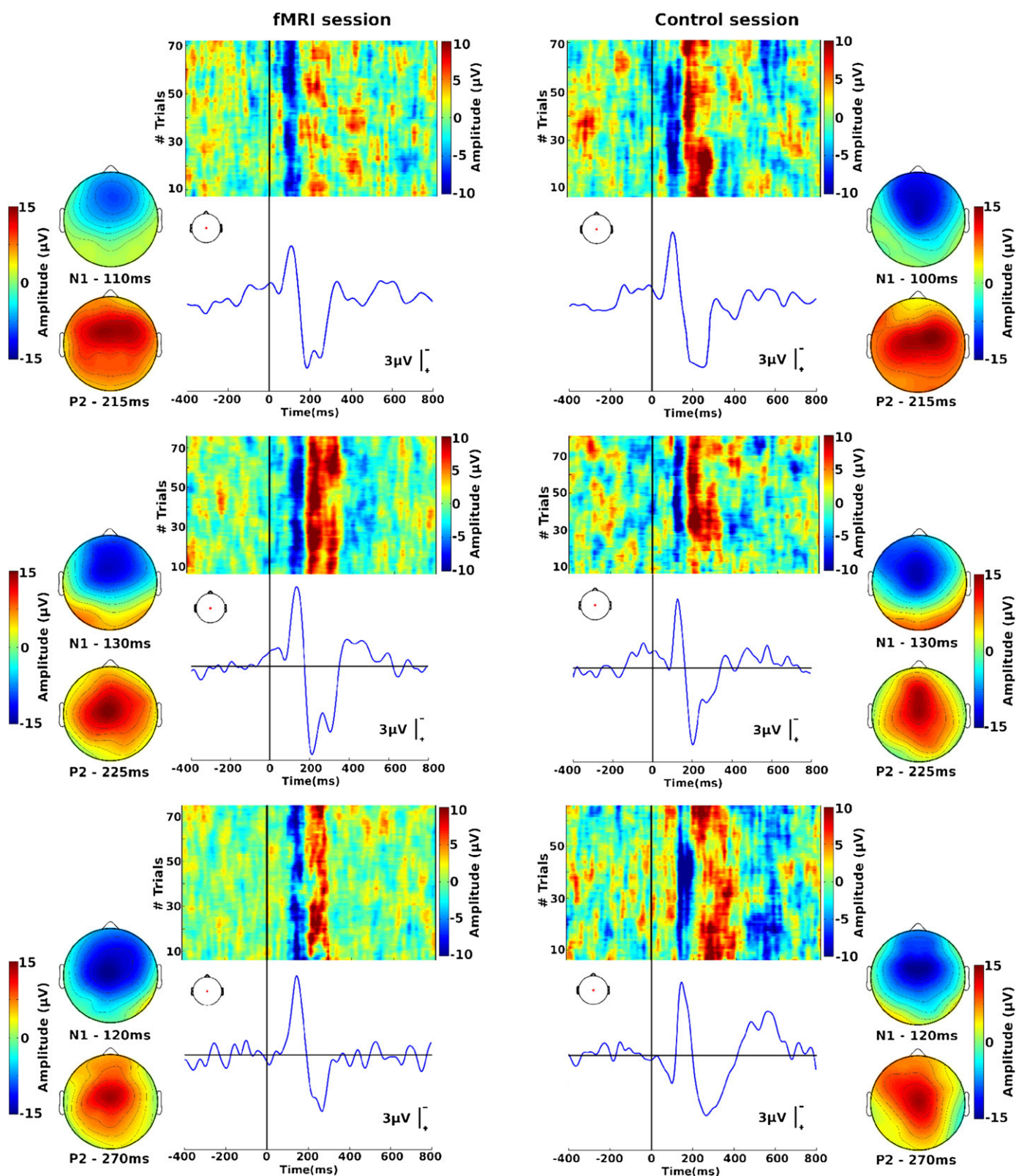
Fig. 4. Reproducibility of single-trial AEP responses. AEPs were recorded during continuous fMRI at 3 T (left column) and in the Control session inside the magnet bore with no fMRI acquisition (right column). Data from three representative subjects are shown here on separate rows. The N1 and P2 peaks recorded from Cz-ref are displayed. To emphasise the high trial-to-trial consistency of the AEP, a bidimensional plot of single-trial responses is shown for each session of each subject. Horizontal lines in each upper-plot represent single-trial responses, with signal amplitude colour coded at each time point. Responses are sorted vertically in order of occurrence, from bottom (first trial) to top (last trial). The waveform below each plot is the average of all single-trial responses for that subject. Voltage negativity is plotted upwards. Beside each waveform are displayed the scalp maps of the electric-field distribution for both N1 and P2 peak, calculated at the same latency to allow comparison between fMRI and Control sessions.

a detection power of 30% for a two-tailed test, $p < 0.05$). The current study would only be expected to detect with a strong power (80% for a two-tailed test, $p < 0.05$) a difference in peak amplitude between sessions that was greater than approximately 3 μV. Therefore, from our results it seems likely that the potential reduction in P2 amplitude during fMRI is less than this.

The trial-to-trial consistency of the main N1 and P2 vertex responses during both the fMRI and Control sessions, is illustrated by sorting single-trial responses vertically in order of occurrence (Fig. 4) for three representative subjects.

Single-trial EEG–BOLD correlations

Fig. 5 displays the mixed-effects group BOLD responses evoked by the mean effect of the auditory stimulus (red–yellow). Brain regions significantly activated in response to the mean effect of the stimulus were found bilaterally in the superior temporal gyrus (STG), middle temporal gyrus, planum temporale, supramarginal gyrus, precentral and postcentral gyri. Significant activation was also observed in the right pallidum, insula, superior frontal gyrus, inferior frontal gyrus, the anterior cingulate gyrus (ACC) and the supplementary motor
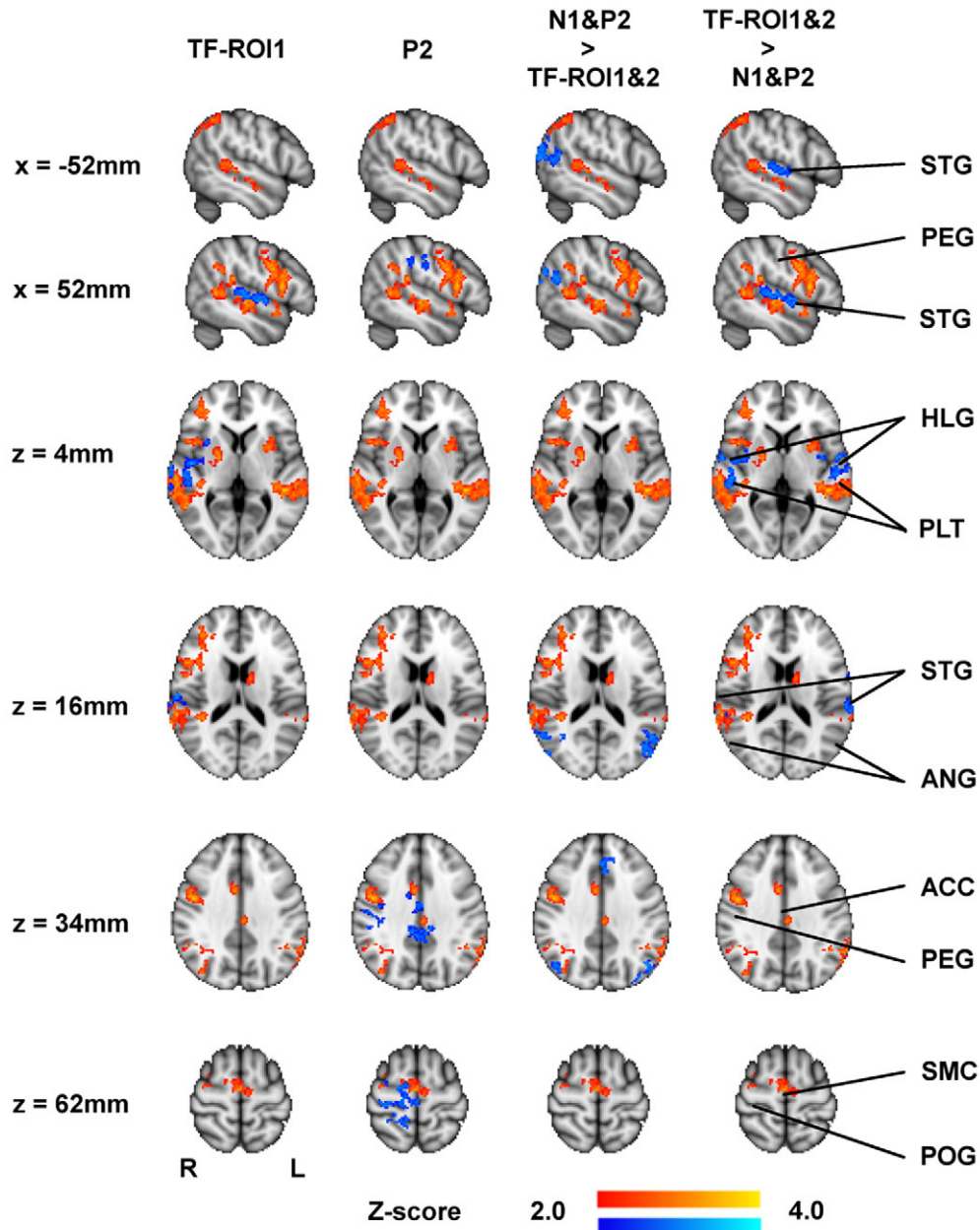

Fig. 5. Group BOLD responses to auditory pure-tone stimulation, and single-trial, single-subject EEG–BOLD correlations. The BOLD response to the mean effect of the stimulus is shown in red–yellow. Overlaid in blue in the first and second columns are the brain regions where the BOLD response was significantly correlated with the single-trial variation in TF-ROI1 amplitude or P2 amplitude respectively. The third and fourth columns display (also in blue) the brain regions where significant results were observed with the Z-contrasts N1 & P2 > TF-ROI1 & TF-ROI2 as well as TF-ROI1 & TF-ROI2 > N1 & P2. Anatomical brain areas are defined as: STG = superior temporal gyrus; PLT = planum temporale; HLG = Heschl's gyrus; PEG = precentral gyrus; POG = postcentral gyrus; ANG = angular gyrus; ACC = anterior cingulate cortex; SMC = supplementary motor cortex. Activation maps are presented for: sagittal slices $x = -52$ and $+52$ mm; axial slices: $z = 62, 34, 16$ and 4 mm. Significant correlations between single-trial TF amplitude in TF-ROI1 and the BOLD response were observed in right STG, PLT and Heschl's gyrus. Significant correlations between single-trial P2 amplitude and BOLD response were observed in pre/postcentral gyrus, the ACC and SMC. Using the additional Z-contrasts, BOLD responses in bilateral auditory areas were shown to be significantly more correlated to TF-ROI1 and TF-ROI2 TF amplitude than to N1 and P2 amplitude. All analysis: mixed-effects, $Z > 2.0$, $p < 0.05$ cluster-corrected.

cortex (SMC). Maximum Z-scores: $Z = 4.4$ on the right side (-44, -36, 2) mm; $Z = 4.2$ on the left side (-46, -36, 2) mm.

Superimposed upon the same selected brain slices (in blue) are the areas where group BOLD responses significantly correlated with the variation in single-trial AEP response derived from P2 amplitude or TF-ROI1 amplitude respectively (Fig. 5). No significant correlation was observed between the BOLD response and N1 amplitude, or TF-ROI2 and TF-ROI3 amplitudes in this voxel-wise analysis.

Significant correlations between single-trial TF amplitude in TF-ROI1 and the BOLD response were observed in right primary (Heschl's gyrus) and secondary (STG, planum temporale) auditory cortex. Significant correlations between single-trial P2 amplitude and BOLD response were observed in precentral and postcentral gyri, cingulate cortex, and the SMC.

We compared BOLD correlations with the time domain and time–frequency domain representations of the main AEP complex (Fig. 5) using the additional Z-contrasts (N1 & P2 > TF-ROI1 & TF-ROI2 as well as TF-ROI1 & TF-ROI2 > N1 & P2), BOLD responses in bilateral auditory areas (Heschl's gyrus, STG and planum tempolare) were shown to be significantly more correlated with TF-ROI1 and TF-ROI2 amplitude than with N1 and P2 amplitude. However, BOLD responses in the angular gyrus and the paracingulate gyrus were observed to be more significantly correlated with N1 and P2 amplitude than with TF-ROI1 and TF-ROI2 amplitude (Fig. 5) on a trial-by-trial basis.

The correlation between the BOLD response and the variation in the five measures of AEP amplitude (N1, P2, TF-ROI1, 2 and 3) was also assessed by examining eight fMRI regions of interest (Fig. 6). The N1 and P2 peak amplitudes did not correlate with the BOLD response in the auditory areas: planum temporale, superior temporal gyrus and Heschl's gyrus. N1 and P2 peak amplitude did correlate with the BOLD response in bilateral precentral and postcentral gyri and the SMC. Additionally P2 correlated with the activity over the amalgamated collection of auditory responsive regions and in the ACC.

The TF amplitude in TF-ROI1 and TF-ROI2 was significantly correlated with the BOLD response in all bilateral auditory areas

investigated (planum temporale, superior temporal gyrus and Heschl's gyrus). In addition TF-ROI1 correlated with BOLD in the precentral gyrus and the ACC. TF-ROI3-BOLD correlations were only observed in the ACC and SMC. No significant correlations were found between BOLD and any of the 5 measures of AEP response in the right putamen or thalamus.

Group mean AEP dipole sources localisation

The results of the dipole localisation of the AEP N1 peak sources can be seen in Supplementary Fig. 3 for both Control and fMRI sessions. Also plotted in white are the boundaries of ellipsoids representing the 95% confidence region of dipole location. The Talairach co-ordinates of the dipoles for Control and fMRI sessions are respectively: Control (± 44, -27, 17) mm; fMRI (± 45, 10, 8) mm. There was a small difference in the dipole location between sessions. The mean AEP during the fMRI session was localised inferior and more lateral than the mean Control session AEP. For both sessions, the dipoles are localised close to the auditory cortex, but slightly superior and medial to the superior temporal gyrus. The confidence ellipsoids indicate that reasonable accuracy has been obtained in localising the source of the group mean AEP response.

Group-level EEG–BOLD correlations

The covariation of the BOLD response with mean N1 and P2 amplitude was also investigated at the group level. Fig. 7A displays the group mean BOLD activation to the auditory stimulus (red) with the BOLD activation found to covary across subjects with mean N1 amplitude (blue) bilaterally in the planum temporale, Heschl's gyrus, superior temporal gyrus, superior frontal gyrus, middle temporal gyrus, right middle frontal gyrus, right supramarginal gyrus, right precentral gyrus and SMC. Results for P2 amplitude are not shown on the brain slices as they appear very similar to N1 covariation across the group.
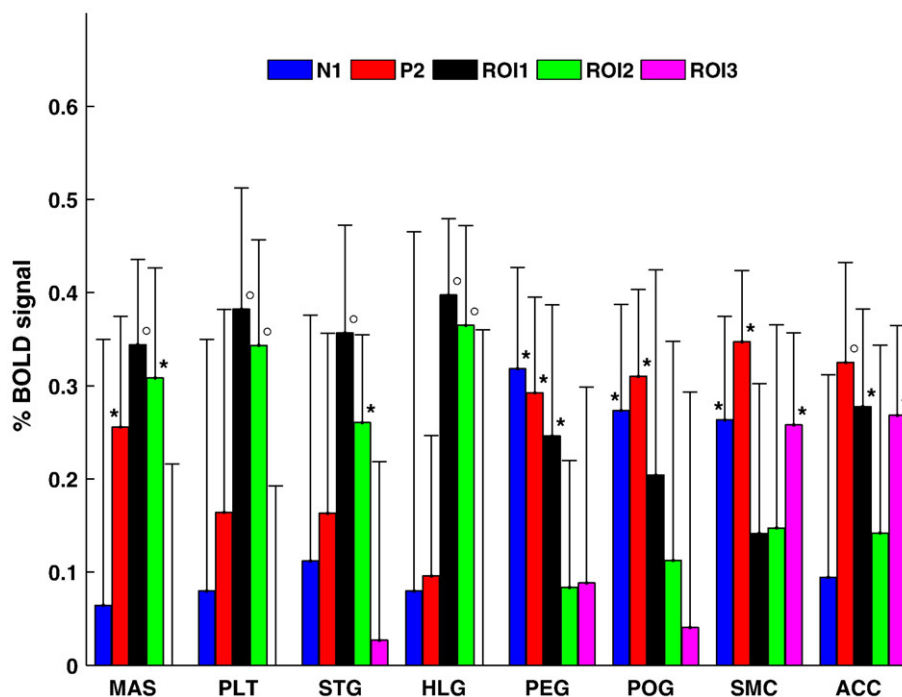
Fig. 6. fMRI-ROI analysis of the BOLD response associated with the time-domain and time–frequency single-trial measures of the AEP response. The mean percentage BOLD signal change calculated from the regression coefficient of the single-trial variation is plotted respectively for: N1 amplitude, P1 amplitude, TF-ROI1, TF-ROI2, TF-ROI3 amplitude in eight functional ROIs: MAS = Mean auditory stimulus; PLT = planum temporale; STG = superior temporal gyrus; HLG = Heschl's gyrus; PEG = precentral gyrus; POG = postcentral gyrus; SMC = supplementary motor cortex; ACC = anterior cingulated cortex. BOLD responses exhibiting a statistically significant difference from zero across the group denoted by * ($p < 0.05$) and ° ($p < 0.01$), two-tailed t-test. Error bars represent ±SEM across subjects.
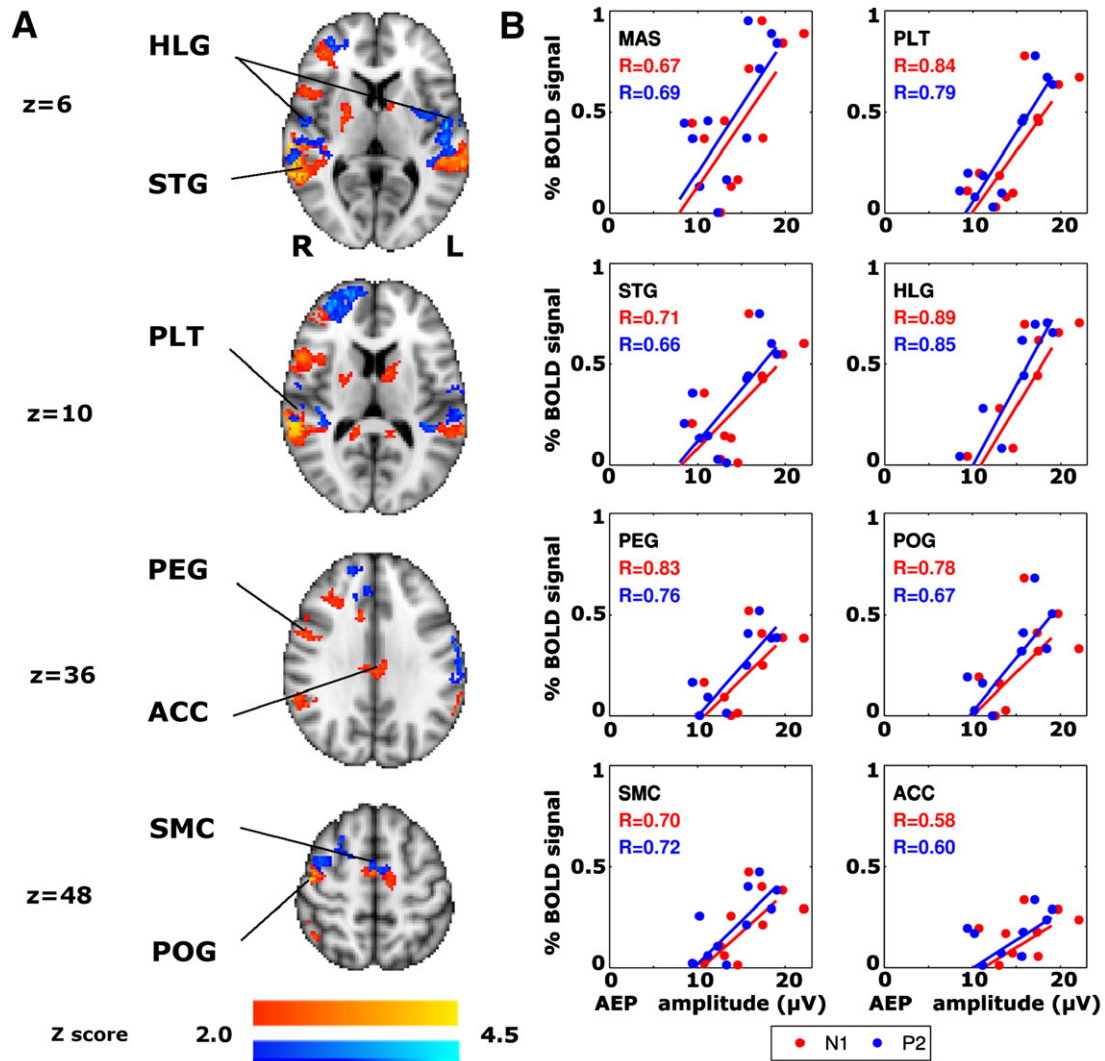
Fig. 7. Group-level correlation between-subjects mean BOLD response and mean amplitude of N1 and P2 AEP peak. (A) Group mean BOLD response to auditory stimulus (red) with the areas where the BOLD response significantly correlated with the group variability in mean AEP N1 superimposed upon selected slices of the MNI standard brain. Significant correlations between-subject N1 amplitude and BOLD response were found bilaterally in the planum temporale, Heschl's gyrus, superior temporal gyrus, superior frontal gyrus, middle temporal gyrus and, right middle frontal gyrus, right supramarginal gyrus, right precentral gyrus and supplementary motor cortex. Mixed-effects, $Z>2.0$, $p<0.05$ cluster-corrected. (B) Functional ROI analysis of the correlation between the BOLD response and the variation subject-mean N1 (red) and P2 (blue) peak amplitude. For each subject, the mean single-trial N1 and P2 amplitude was correlated with the mean percent BOLD signal change in each of the eight functional ROIs. MAS = Mean auditory stimulus; PLT = planum temporale; STG = superior temporal gyrus; HLG = Heschl's gyrus; PEG = precentral gyrus; POG = postcentral gyrus; SMC = supplementary motor cortex; ACC = anterior cingulate cortex. In all displayed plots, BOLD responses exhibited a statistically significant correlation with both N1 and P2 amplitude across the group $p<0.05$.

The correlation between the mean single-trial amplitude of each subject's N1 and P2 peak and BOLD response was also assessed with an ROI analysis in 8 auditory responsive regions defined above (Fig. 7B). Significant positive BOLD responses that correlated with subjects' mean N1 and P2 amplitude were observed in all eight functional ROIs displayed ($p<0.05$, two-tailed t-test uncorrected): MAS = Mean auditory stimulus; PLT = planum temporale; STG = superior temporal gyrus; HLG = Heschl's gyrus; PEG = precentral gyrus; POG = postcentral gyrus; SMC = supplementary motor cortex; ACC = anterior cingulate cortex.

Discussion

We have successfully demonstrated the simultaneous acquisition of auditory-evoked potentials with continuous BOLD fMRI at 3 T. The primary negative and positive peaks (N1 and P2) of the vertex potential of the AEP were well preserved during fMRI compared to the Control recording sessions (without MRI gradient acoustic and

electrical noise). While N1 appeared to be unaffected by fMRI, there was a trend towards a reduction in amplitude of the later P2 potential. We have used our 30 channel EEG recordings to demonstrate that the scalp distribution of AEPs between fMRI and Control sessions was qualitatively similar. In addition, the bilateral locations of N1 dipole sources were shown to be comparable between fMRI and Control sessions, close to the auditory cortex. The data suggests that no substantial degrading effect on the AEP is introduced by performing continuous, simultaneous EEG–fMRI of this basic auditory stimulus. In the present study, the acquisition of AEPs during continuous fMRI that are not substantially attenuated by the gradient acoustic noise can be partly (anecdotally) attributed to the use of within-ear stimulus delivery combined with MR-acoustic noise reduction via ear defenders. We observed BOLD activation evoked by the auditory stimulus that was consistent with previous reports of brain activity during processing of pure-tone stimulation (Mulert et al., 2004; Benar et al., 2007), in bilateral auditory cortical areas including the planum temporale and superior temporal gyrus as well as bilateral precentral

and postcentral gyri. BOLD responses that covaried with the single-trial measures of AEP amplitude were also found in these brain areas. The BOLD response in primary auditory cortex (Heschl's gyrus) did not reach (cluster-corrected) statistical significance. This may result from the constant acoustic MR noise was present throughout the experiment causing a response saturation in primary auditory areas (Langers et al., 2005).

Quality of EEG responses recorded during fMRI and Control sessions

Our study was motivated by further investigating the feasibility of recording AEPs during continuous fMRI. Novitski et al. (2001) demonstrated that recorded MRI noise does not have a significant effect on the amplitude of the N1 or the P2 peak of the AEP. While our results are in broad agreement, in the present study a non-significant reduction in the amplitude of the P2 peak was observed during fMRI, potentially arising from the effects of acoustic scanner noise. Previous studies have shown that evoked-potential peaks which occur at longer latencies exhibit a greater tendency to be modulated by attentional mechanisms (Salmi et al., 2007; Wronka et al., 2007). We also observed a very late negative potential, occurring approximately 600 ms post-stimulus in the Control session. Late peaks occurring around and later than 300 ms post-stimulus are often studied in cognitive experiments investigating memory and perception of deviant stimuli. The amplitude of these peaks is larger when stimuli are infrequently presented. Taking the MR noise into account, it is likely that stimuli presented in a Control session would appear more salient than auditory stimuli presented during fMRI scanning, which might explain the difference in amplitude of this N600 between sessions. It should also be noted that the present study has used a simple, single-frequency (1 kHz), auditory stimulus. The perception of the stimulus and the possible interaction of stimulus and scanner noise will be different for complex auditory stimuli such as a speech or modulated multi-frequency tones.

The EEG data acquired during fMRI was acquired under conditions of high acoustic noise combined with the presence of gradient artifacts in the EEG. A recent study has shown that EEG data may be degraded in some circumstances by the use of gradient artifact correction algorithms (Groullier et al., 2007). In this study we evaluated the gradient artifact removal algorithm FASTR upon AEPs from the Control sessions of three representative subjects. We believe that these simulations have demonstrated that FASTR processing has, at worst, a very minor effect on the shape and amplitude of the AEP waveforms recorded in this study. Based on these results we conclude that the use of FASTR for MR-artifact removal does not significantly affect the amplitudes of the AEPs recorded during fMRI compared to the AEPs recorded during the Control session.

A recent study has shown that the amplitude, latency and scalp distribution of the N2–P2 vertex potential of A-δ mediated laser-evoked potentials (LEPs) recorded simultaneously with fMRI, were almost identical to LEPs recorded in a separate session outside the fMRI scanner (Iannetti et al., 2005). Further studies have shown that the data quality of visual evoked potentials during interleaved EEG–fMRI recording is not superior to recordings performed during continuous fMRI acquisition (Becker et al., 2005; Warbrick and Bagshaw, 2008). A comparison of pre-processed EEG data from Control and fMRI sessions is given for the present study in Supplementary Fig. 1.

In the time domain, the difference between the N1 and P2 amplitudes measured from the group average ERP compared to the mean single-trial measurements (Figs. 2, 3 and Table 1), can be attributed to the non-stationarity of the AEP across trials. Averaging non-stationary evoked-potential signals is in effect averaging signals with inconsistent phase. This causes a distortion of the waveform and decreases the amplitude of the average away from its true value. This can be ameliorated by adopting the single-trial analysis as previously demonstrated (Mayhew et al., 2006).

In this study we used wavelet transforms and subject-specific PCA decompositions of single-trial AEPs to define the three most consistent components of transient, oscillatory power changes in the time–frequency domain (Fig. 1). The TF-ROI technique allowed a novel, alternative conceptualisation, compared to N1 and P2 vertex measures, in identifying the significant frequency components of the AEP, and the subsequent correlation of different frequency components with the simultaneously acquired BOLD response. An increase in time–frequency amplitude in the delta-theta frequency range that was centered around the AEP latency is attributed to the time–frequency representation of the ERP (TF-ROI1). A region of ERS was identified immediately post-stimulus that corresponded to the theta-alpha frequency range (TF-ROI2). In addition a third region of ERD was observed in the theta-alpha range beginning 500 ms post-stimulus.

Sources of auditory activity

Auditory-evoked potentials recorded at latencies greater than 50 ms post-stimulus are called late AEPs (Picton et al., 1974). The auditory N1 peak is itself composed of several anatomically and functionally distinct subcomponents. Three subcomponents, all with a peak latency of approximately 100 ms, have been reported. Two of these are thought to originate from temporal cortical areas and the third, hypothesised to reflect a widespread transient arousal originating in frontal cortex, is probably generated by the ACC. A dipole source analysis of the N1 peak has shown that it originates bilaterally from the supratemporal plane of the auditory cortex, but also from bilateral frontal regions hypothesised to be located in either cingulate or supplementary motor areas (Giard et al., 1994). Contributions to the P2 peak are also believed to originate from neural activity in the temporal lobe, but like the N1, dipole modelling studies report multiple source solutions. MEG recordings (Godey et al., 2001) have suggested that the generators of the P2 peak are located in the planum temporale and the auditory association complex. Contributions from secondary somatosensory cortex (SII) are also speculated (Hari et al., 1980). These AEP source localisation studies demonstrate a contribution of the ACC and postcentral gyrus/SII. We observed these regions to display a BOLD activation correlated with variability in individual AEP amplitude (Figs. 5–7).

The present study was designed to focus on extracting temporal and frequency domain features of the vertex potential, rather than source localisation of multi-channel EEG data. However, it is interesting to compare source localisations of AEP responses with the locations of fMRI activations. The results of our dipole modeling suggest bilateral sources superior and medial to the fMRI activations measured in the superior temporal gyrus. Previous EEG–fMRI studies have localised the N1 AEP peak with bilateral dipoles or current source density maps in auditory cortex (Mulert et al., 2004; Scarff et al., 2004a; Debener et al., 2007a,b). However, in support of our dipole localisations previous EEG–fMRI study found that the fMRI and AEP dipole localisation agreed within the horizontal plane but reported a significant systematic difference in the vertical plane (Scarff et al., 2004a).

We believe that our dipole results compare favorably to those in previous studies especially considering we recorded from only 30 electrodes compared to over 60 in those studies (Scarff et al., 2004a; Debener et al., 2007a,b). The small displacement of our dipole sources could be explained by a lack of spatial information due to spare scalp coverage of 30 electrodes. In particular, when using 30 electrodes in a 10/20 montage, almost all electrodes are positioned at scalp locations above the auditory cortex, a bias that could be the determining factor for the vertical mislocation. It is suggested that that the recording montage should include electrodes placed on the neck, face, and lower scalp to record the activity over the lower half of the spherical conductor to prevent the zero-line of the average-reference data from being shifted upwards (Scarff et al., 2004a).

Single-trial EEG–fMRI correlations and their functional implications

Recently, Benar et al. (2007) conducted the first continuous, simultaneous EEG–fMRI study of auditory oddball stimuli at 3 T. That study supports our findings that the variability in single-trial AEP responses contains significant meaningful information that correlate with the variation in the simultaneously acquired BOLD signal.

In the present study, BOLD responses that correlated with the single-trial, within-session amplitude measures of the AEP in primary (Heschl's gyrus) and secondary auditory cortex (STG and planum temporale) were observed preferentially with TF-ROI1 and TF-ROI2 rather than the more conventional N1 and P2 amplitude measures of the AEP. In contrast, P2 peak amplitude and BOLD response correlations were observed in right pre- and postcentral gyri, the cingulate cortex and SMC (Fig. 5). No significant N1–BOLD correlations were observed using a voxel-wise analysis. This result can be partly explained by the substantial covariation between N1 and P2 amplitudes. Despite the different cortical generators of these AEP peaks, the N1 and P2 amplitude measures share some inherently common variance, and in this study the P2 peak amplitude has been shown to be more significantly correlated with the BOLD fMRI response. The fact that the fMRI analysis driven by estimated amplitude of the auditory ERP response failed to identify a brain response in primary auditory regions is in agreement with some recent experimental evidence indicating that much of the ERP elicited by stimuli of different sensory modalities (including auditory) could be explained by neural activity which is not modality-specific (i.e. uniquely elicited by stimuli of a single sensory modality), but instead is multimodal (i.e. elicited by stimuli belonging to different sensory modalities). This may support the notion that sensory ERPs, or at least trial-to-trial variability in sensory ERPs, are mostly related to the saliency of the eliciting stimulus (Iannetti et al., 2008, Mouraux and Iannetti, 2009). The contribution of these multimodal activities, which in source analysis are optimally modeled by both opercular and deep midline dipoles, becomes dominant at the latency of the P2 wave, and thus it is not surprising that the single-trial EEG–fMRI correlations performed in the present study, such as that with TF-ROI3 yielded neural responses in the cingulate cortex. Thus the variability in activity associated with TF-ROI3 (Fig. 6) may represent post-stimulus alerting or an attentional shift differing from trial to trial.

In Fig. 5 we demonstrate by using fMRI contrasts of TF-ROI1 & TF-ROI2>N1 & P2 that BOLD activity in the bilateral primary auditory cortex correlates more significantly with the EEG response measured using TF-ROIs than with measures derived from time-domain amplitudes. Our results suggest therefore that the different measures of the AEP response are predictive of different regional BOLD responses. Single-trial measures derived from TF-ROIs were the only predictor that identified the involvement of primary auditory cortex (Heschl's gyrus) in processing the auditory stimuli. By correlating TF-ROI amplitudes with the fMRI response we have also revealed significant EEG-correlated BOLD activity in the STG and planum temporale which were areas activated by the main effect of the auditory stimulus. No significant voxel-wise correlations were observed between the BOLD response and the single-trial N1 or P2 amplitudes in auditory cortices. This finding, besides confirming the notion that the time-domain ERP response elicited by sensory stimuli mostly reflects non-modality-specific processes, suggests that more sensory-specific, percept-related neural processing of incoming stimuli might be reflected in more subtle, non-phase-locked transient variations of EEG oscillatory activities (Makeig et al., 2002; Mouraux et al., 2003; Mouraux and Iannetti, 2008).

The only significant correlations between BOLD and P2 amplitude were found in the left precentral and postcentral gyri, the SMC and the ACC. All these areas were also observed to possess a BOLD response evoked by the mean effect of the stimulus (Fig. 5). This network of cortical areas where the BOLD response amplitude was observed to

covary with the AEP response may be associated with maintaining attention to the stimulus and the cognitive demand of distinguishing the auditory tone from the background MR noise, rather than modality-specific auditory responses. The single-trial correlations of P2 amplitude with the BOLD response in cingulate cortex is in good agreement with the existing literature describing the cortical sources of the time-domain AEP.

Our time–frequency analysis has enabled us to show that EEG responses in both the theta (2–5 Hz) and theta-alpha frequency (6–15 Hz) ranges contain information about activity in the auditory cortex. This result suggests firstly that time–frequency techniques may provide improved signal-to-noise for measurement of evoked potential amplitudes. Secondly, these results illustrate the ability of a time–frequency analysis to reveal significant non-phase-locked, event-related activity beyond what is measured by an analysis restricted to the time domain. To the authors' knowledge this is the first time a single-trial time–frequency ROI analysis has been used to demonstrate correlations between the amplitudes of simultaneously acquired EEG–fMRI measured brain responses. Animal studies and human fMRI studies have revealed that sound-level dependence is present only in the primary auditory cortices and not the secondary auditory cortices (Juckel et al., 1996; Brechmann et al., 2002; Hart et al., 2003). Correlations between the 3–6 Hz power of EEG responses to speech perception have recently been shown to significantly correlate with the BOLD response in right Heschl's gyrus (Giraud et al., 2007), in broad agreement with our observed correlation in TF-ROI1 lying mainly in the 2–5 Hz range.

Group-level EEG–fMRI correlations

At the group level, BOLD activation that correlated with across-subject variation in N1 amplitude was found bilaterally in the planum temporale, Heschl's gyrus, superior temporal gyrus, middle temporal gyrus, precentral gyrus, the SMC and in the right prefrontal cortex (Fig. 7A). These results suggest that subjects with a larger AEP response have a generally larger BOLD response in regions responding to the stimulus, supporting the notion that the neurophysiological origins of the two measurements are strongly linked (Arthurs et al., 2000; Mukamel et al., 2005; Logothetis et al., 2001). The modulation of ACC and SII activity suggests a representation of differing subject attention and a modulation of cognitive processing involved in perceiving the stimulus. It is known that the amplitude of evoked potentials can be significantly modulated by attention (Arthurs et al., 2004). In all regions of interest, BOLD responses significantly correlated with subject-mean N1 and P2 amplitudes (Fig. 7B), with the stronger effect being observed for P2. Subjects with a larger evoked potential tended to give a stronger BOLD response across a wide network of brain areas, suggesting either a greater degree of neuronal activity for a given stimulus or a larger stimulus input i.e. more sound energy stimulating acoustic receptors, or a combination of both. True equalisation across subjects of the sound energy reaching the inner ear from the stimulus compared to that from MR scanner noise is difficult to achieve because of differences in individual anatomy of participants. Activation in auditory cortices that correlated with across-subject AEP variability may be related to the qualities of the auditory stimulus, such as its perceived loudness. Fig. 7B suggests that a BOLD response would not be detectable in volunteers whose AEP (N1 or P2) is less than about 10 μV, suggesting that the EEG may be more sensitive than the BOLD signal for detecting auditory activity in the chosen task.

Advantages and disadvantages of simultaneous EEG–fMRI

Many studies recording evoked potentials and fMRI have adopted an interleaved approach, either alternating relatively long periods of fMRI acquisition with similar periods without fMRI scanning

(Bonmasser et al., 2001; Liebenthal et al., 2003; Scarff et al., 2004a; Thaerig et al., 2007), or performing *sparse* fMRI, i.e., collecting single images with a delay that allows the registration of the predicted peak of an evoked hemodynamic response (Christmann et al., 2002; Kruggel et al., 2001). In either case, EEG recording is carried out during a time-window free from MR noise and gradient switching, thus avoiding the MR imaging artifact on the recorded EEG and the potential acoustic masking on the perception of the stimulus.

Our results show that reliable AEPs can be recorded also when EEG and fMRI are collected at the same time, and this truly simultaneous multimodal recording avoids the important theoretical and practical limitations of the interleaved approach. First, when long periods of EEG acquisition are interleaved with long periods of fMRI scanning, the two techniques do not sample the same neural phenomenon. Second, even when *sparse* image collection is performed, the hemodynamic response is not densely sampled leading to greater uncertainty during its modelling (Garreffa et al., 2004; Nebel et al., 2004). The interleaved design reduces the flexibility in the stimulus presentation paradigm and increases the overall duration of the experiment. Long scan times also risk increasing volunteer discomfort and increasing the risk of time-dependent variations of the cognitive state of the subject such as attention. The ability to acquire continuous simultaneous blocks of AEPs enables the stimulus to be inter-woven with delivery paradigms including other stimuli, without compromising the design of those studies.

The integration of EEG–fMRI data using a linear prediction model as used in the present study makes the assumption that the data recorded from a scalp EEG channel is related to the fMRI activation in single fMRI voxels. Recently, several other simultaneous EEG–fMRI studies have successfully employed single-trial analysis of evoked potentials arising from auditory oddball, error detection, and contingent negative variation stimuli as predictors of the BOLD response. These studies successfully identified aspects of the fMRI activity that covary with the variability in the electrophysiological response (Nagai et al., 2004, Debener et al., 2005, Eichele et al., 2005; Benar et al., 2007). The demonstration of correlations between EEG and fMRI signals does not necessarily imply that the signals have the same underlying physiological source. However, use of a trial-by-trial EEG marker has the potential to help us find correlated fMRI activity that varies from trial-to-trial, which may not be the direct source of the EEG signal but which may be an important part of the system engaged in the generation. Indeed, we report regions of fMRI signal correlation with the vertex AEP that are spatially separated from the cortical regions identified by our dipole modeling.

Evoked potentials are a stimulus induced, transient change in the ongoing EEG signal, created by time-locked neural activities over a relatively small time window. They reflect the summation of synchronously active and spatially aligned cortical pyramidal cells (Speckmann and Elger, 2004), and in addition are sensitive to the dendrite orientation, conduction through the brain and skull, and the possible cancellation of opposing current sources in a complex anatomical location such as the superior temporal gyrus. The AEPs recorded in this study are therefore a limited representation of the total neural activity at any given instant from the auditory processing. In contrast, the BOLD fMRI signal integrates time-locked and non-time-locked neural activities from the entire neuronal population regardless of the orientation, or excitatory or inhibitory designation of those neurons (Logothetis et al., 2001). The different physiological origins of the EEG and BOLD signals could provide a further reason for the difference in location of fMRI activity and the modeled dipole sources of the AEP observed in this study.

Furthermore, very recent work using probabilistic ICA has presented evidence that evoked-potential responses to auditory, visual, somatosensory and nociceptive stimulation represent considerable neural activity from brain areas that are not processing that specific sensory input. This finding suggests that auditory-specific components may form only a relatively small part of the total AEP signal, with large components being generated from higher cortical areas (Mouraux and Iannetti, 2009). This study is one of several to demonstrate that auditory evoked BOLD fMRI responses in higher cortical areas such as the ACC, supplementary motor cortex and pre- and postcentral gyri, in addition to bilateral auditory cortex (Mulert et al., 2004; Benar et al., 2007).

The aim of the current study was to exploit the extra temporal information provided by combining EEG with fMRI recordings and investigate correlations between the EEG and BOLD responses. We did not find correlations between the N1 or P2 waveform amplitude and the BOLD response in auditory cortex. However, we have provided evidence that some components of the activity underlying the N1 peak originate from close to the auditory cortex. We feel that this result provides a validation of our data quality. One of the primary findings of this study was the correlation between TF-ROI1 amplitude and the BOLD signal in auditory cortex. This result demonstrates that our TF-ROI analysis of single-trial AEPs has provided us with additional sensitivity over an analysis based upon simple time-domain waveforms.

The exact nature of the relationship between EEG and fMRI neuroimaging measurements requires much further investigation despite several reports of correlations between EEG and fMRI signals (Arthurs et al., 2000; Debener et al., 2005; Eichele et al., 2005; Benar et al., 2007). Simultaneous recording of EEG and fMRI is necessary when spontaneous alterations of electrophysiological activity are under investigation. Under such circumstances simultaneous recording of EEG and fMRI provides us with the tool to undertake these investigations to identify specific relationships between EEG and fMRI measures of brain activity.

Acknowledgments

Appendix A. Supplementary data

Supplementary data associated with this article can be found, in the online version, at doi:10.1016/j.neuroimage.2009.06.080.

References

Adeli, H., Zhou, Z., Dadmehr, N., 2003. Analysis of EEG records in an epileptic patient using wavelet transform. J. Neurosci. Methods 123 (1), 69–87.

Arthurs, O.J., Williams, E.J., Carpenter, T.A., Pickard, J.D., Boniface, S.J., 2000. Linear coupling between functional magnetic resonance imaging and evoked potential amplitude in human somatosensory cortex. Neuroscience 101 (4), 803–806.

Arthurs, O.J., Johansen-Berg, H., Matthews, P.M., Boniface, S.J., 2004. Attention differentially modulates the coupling of fMRI BOLD and evoked potential signal amplitudes in the human somatosensory cortex. Exp. Brain. Res. 157 (3), 269–274.

Bandettini, P.A., Jesmanowicz, A., Van Kylen, J., Birn, R.M., Hyde, J.S., 1998. Functional MRI of brain activation induced by scanner acoustic noise. Magn. Reson. Med. 39, 410–416.

Basar, E., Demiralp, T., Schurmann, M., Basar-Eroglu, C., Ademoglu, A., 1999. Oscillatory brain dynamics, wavelet analysis and cognition. Brain Lang. 66, 146–183.

Belin, P., Zattorre, R.J., Hoge, R., Evans, A.C., Pike, B., 1999. Event-related fMRI of the auditory cortex. NeuroImage 10, 417–429.

Bell, A., Sejnowski, T., 1995. An information-maximization approach to blind signal separation and blind deconvolution. Neural. Comput. 7, 1129–1159.

Becker, R., Ritter, P., Moosmann, M., Villringer, A., 2005. Visual evoked potentials recovered from fMRI scan periods. Hum. Brain Mapp. 26, 221–230.

Benar, C.G., Schon, D., Grimault, S., Nazarian, B., Burle, B., Roth, M., Badier, J.M., Marquis, P., Liegeois-Chavel, C., Anton, J.L., 2007. Single-trial analysis of oddball event-related potentials in simultaneous EEG-fMRI. Hum. Brain Mapp. 28, 602–613.

Bernat, E.M., Williams, W.J., Gehring, W.J., 2005. Decomposing ERP time–frequency energy using PCA. Clin. Neurophysiol. 116, 1314–1334.

Bernat, E.M., Malone, S.M., Williams, W.J., Patrick, C.J., Iacono, W.G., 2007. Decomposing delta, theta and alpha time–frequency ERP activity from a visual oddball task using PCA. Int. J. Psychophysiology 64, 62–74.

Bonmasser, G., Schwartz, D.P., Liu, A.K., Kwong, K.K., Dale, A.M., Belliveau, J.W., 2001. Spatiotemporal brain imaging of visual-evoked activity using interleaved EEG and fMRI. NeuroImage 13, 1035–1043.

Brechmann, A., Baumgart, F., Scheich, H., 2002. Sound-level-dependent representation of frequency modulations in human auditory cortex, a low noise fMRI study. J. Neurophysiol. 87, 423–433.

Busch, N.A., Debener, S., Kranczioch, C., Engel, A.K., Herrmann, C.S., 2004. Size matters, effects of stimulus size, duration and eccentricity on the visual gamma-band response. Clin. Neurophysiol. 115 (7), 1810–1820.

Cacace, A.T., McFarland, D.J., 2003. Spectral dynamics of electroencephalographic activity during auditory information processing. Hearing Res. 176, 25–41.

Cho, Z.H., Chung, S.C., Lim, D.W., Wong, E.K., 1998. Effects of the acoustic noise of the gradient systems on fMRI, a study on auditory, motor and visual cortices. Magn. Reson. Med. 39, 331–336.

Christmann, C., Ruf, M., Braus, D.F., Flor, H., 2002. Simultaneous electroencephalography and functional magnetic resonance imaging of primary and secondary somatosensory cortex in humans after electrical stimulation. Neurosci. Lett. 333, 69–73.

Debener, S., Ullsperger, M., Siegel, M., Fiehler, K., von Cramon, D.Y., Engel, A.K., 2005. Trial-by-trial coupling of concurrent electroencephalogram and functional magnetic resonance imaging identifies the dynamics of performance monitoring. J. Neurosci. 25 (50), 11730–11737.

Debener, S., Strobel, A., Sorger, B., Peters, J., Kranczioch, C., Engel, A.K., Goebel, R., 2007a. Improved quality of auditory event-related potentials recorded simultaneously with 3-T fMRI, removal of the ballistocardiac artefact. NeuroImage 34 (2), 587–597.

Debener, S., Ullsperger, M., Siegel, M., Engel, A.K., 2007b. Towards single-trial analysis in cognitive brain research. Trends Cogn. Sci. 11 (12), 502–503.

Delorme, A., Makeig, S., 2004. EEGLAB: an open source toolbox for analysis of single-trial EEG dynamics including independent component analysis. J. Neurosci. Methods. 131 (921).

Demiralp, T., Yordanova, J., Kolev, V., Ademoglu, A., Devrim, M., Savar, V.J., 1999. Time–frequency analysis of single-sweep event-related potentials by means of fast Fourier transform. Brain Lang. 66, 129–145.

Di Salle, F., Esposito, F., Scarabino, T., Formisano, E., Marciano, E., Saulino, C., Cirillo, S., Elefante, R., Scheffler, K., Seifritz, E., 2003. fMRI of the auditory system: understanding the basis of auditory gestalt. Magn. Reson. Imaging. 21 (10), 1213–1224.

Edmister, W.B., Talavage, T.M., Ledden, P.J., Weiskoff, R.M., 1999. Improved auditory cortex imaging using clustered volume acquisitions. Hum. Brain Mapp. 7, 89–97.

Eichele, T., Specht, K., Moosmann, M., Jongsma, M.L.A., Quian Quiroga, R., Nordby, H., Hugdahl, K., 2005. Assessing the spatiotemporal evolution of neuronal activation with single-trial event-related potentials and functional MRI. Proc. Nat. Acad. Sci. U. S. A. 102 (6), 17798–17803.

Elliot, M.R., Bowtell, R.W., Morris, P.G., 1998. The effect of scanner sound in visual, motor and auditory functional MRI. Magn. Reson. Med. 41, 1230–1235.

Garreffa, G., Bianciardi, M., Hagberg, G.E., Macaluso, E., Marciani, M.G., Maraviglia, B., Abbafati, M., Carni, M., Bruni, I., Bianchi, L., 2004. Simultaneous EEG/fMRI acquisition, how far is it from being a standardised technique? Magn. Reson. Imaging 22, 1445–1455.

Giard, M.H., Perrin, F., Echallier, J.F., Thevanet, M., Froment, J.C., Pernier, J., 1994. Dissociation of temporal and frontal components in the human auditory N1 wave, a scalp current density and dipole model analysis. Electroencephalogr. Clin. Neurophysiol. 92, 238–252.

Giraud, A.L., Kleinschmidt, A., Poeppel, D., Lund, T.E., Frackowiak, R.S.J., Laufs, H., 2007. Endogenous cortical rhythms determine cerebral speech specialisation for speech perception and production. Neuron 56, 1127–1134.

Godey, B., Schwartz, D., de Grall, J.B., Chauvel, P., Liegeois-Chauvel, C., 2001. Neuromagnetic source localization of auditory evoked fields and intracerebral evoked potentials, a comparison of data in the same patients. Clin. Neurophysiol. 112, 1850–1859.

Goldmann, R.I., Stern, J.M., Engel Jr., J., Cohen, M.S., 2002. Simultaneous EEG and fMRI of the alpha rhythm. NeuroReport 13, 2487–2492.

Gotman, J., 2008. Epileptic networks studied with EEG–fMRI. Epilepsia 49 (3), 42–51.

Groullier, F, Vercueil, L, Krainik, A, Segebarth, C, Kahane, P, David, O., 2007. A comparative study of different artifact removal algorithms for EEG signals acquired during functional MRI. NeuroImage 38, 124–137.

Hall, D.A., Summerfield, A.Q., Goncalves, M.S., Foster, J.R., Palmer, A.R., Bowtell, R.W., 2000. Time-course of the auditory BOLD response to scanner noise. Magn. Reson. Med. 43, 601–606.

Hari, R., Aittoniemi, K., Jarvinen, M.L., Katila, T., Varpula, T., 1980. Auditory evoked transient and sustained magnetic fields of the human brain. Localisation of neural generators. Exp. Brain Res. 40, 237–240.

Hart, H.C., Hall, D.A., Palmer, A.R., 2003. The sound-level-dependent growth in the extent of fMRI activation in Heschl's gyrus is different for low- and high-frequency tones. Hearing Res. 179, 104–112.

Iannetti, G.D., Wise, R.G., 2007. BOLD functional MRI in disease and pharmacological studies, room for improvement? Mag. Reson. Med. 25 (6), 978–988.

Iannetti, G.D., Niazy, R.K.N., Wise, R.G., Jezzard, P., Brooks, J.C.W., Zambreanu, L., Matthews, P.M., Tracey, I., 2005. Simultaneous recording of laser-evoked brain potentials and continuous, high-field functional magnetic resonance imaging in humans. NeuroImage 28 (3), 708–719.

Jenkinson, M., Smith, S., 2001. A global optimization method for robust affine registration of brain images. Med. Image Anal. 5, 143–156.

Jenkinson, M., Bannister, P., Brady, M., Smith, S., 2002. Improved optimisation for the robust and accurate linear registration and motion correction of brain images. NeuroImage 17, 825–841.

Juckel, G., Csepe, V., Molnar, M., Hegerl, U., Karmos, G., 1996. Intensity dependance of auditory evoked potentials in behaving cats. Electroencephalogr. Clin. Neurophysiol. 100, 527–537.

Kruggel, F., Herrmann, C.S., Wiggings, C.J., Von Cramon, D.Y., 2001. Hemodynamic and electroencephalographic responses to illusory figures, recording of the evoked potentials during functional MRI. NeuroImage 14, 1327–1336.

Langers, D.R., Van Dijk, P., Backes, W., 2005. Interactions between hemodynamic responses to scanner acoustic noise and auditory stimuli in functional magnetic resonance imaging. Mag. Reson. Med. 53 (1), 49–60.

Laufs, H., Kleinschmidt, A., Beyerle, A., Eger, E., Salek-Haddadi, A., Preibisch, C., Krakow, K., 2003. EEG-correlated fMRI of human alpha activity. NeuroImage 19, 1463–1476.

Liebenthal, E., Ellingson, M.L., Spanaki, M.V., Prieto, T.E., Ropella, K.M., Binder, J.R., 2003. Simultaneous ERP and fMRI of the auditory cortex in a passive oddball paradigm. NeuroImage 19, 1395–1404.

Logothetis, N.K., Pauls, J., Augath, M., Trinath, T., Oeltermann, A., 2001. Neurophysiological investigation of the basis of the fMRI signal. Nature 412, 150–157.

Krause, C.M., 1999. Event-related EEG changes during auditory processing. In: Pfurtscheller, G., Lopes da Silva, F.H. (Eds.), Event-Related Desynchronisation, Vol 6. Elsevier, Amsterdam., pp. 195–201.

Makeig, S., Westerfield, M., Jung, T.P., Enghoff, S., Townsend, J., Courchesnse, E., Sejnowski, T.J., 2002. Dynamic brain sources of visual evoked responses. Science 295, 690–694.

Makinen, V., Tiitinen, H., May, P., 2004. Human auditory event-related processes in the time–frequency plane. NeuroReport 15 (11), 1767–1771.

Mayhew, S.D., Iannetti, G.D., Woolrich, M.W., Wise, R.G., 2006. Automated single-trial measurement of amplitude and latency of laser-evoked potentials (LEPs) by multiple-linear regression. Clin. Neurophysiol. 117, 1331–1344.

Moosmann, M., Ritter, P., Krastel, I., Brink, A., Thees, S., Blankenberg, F., Taskin, B., Obrig, H., Villringer, A., 2003. Correlates of alpha rhythm in functional magnetic resonance imaging and near infrared spectroscopy. NeuroImage 20, 145–158.

Mouraux, A., Iannetti, G.D., 2008. Across-trial averaging of event-related responses and beyond. Magn. Reson. Imag. 26 (7), 1041–1054.

Mouraux, A., and Iannetti, G.D., 2009. Nociceptive laser-evoked brain potentials do not reflect nociceptive-specific neural activity. J. Neurophysiology101, 3258–3269.

Mouraux, A., Guerit, J.M., Plaghki, L., 2003. Non-phase locked electroencephalogram (EEG) response to CO2 laser skin stimulations may reflect central interactions between Aδ and C-fibre afferent volleys. Clin. Neurophysiol. 114, 710–722.

Mulert, C., Jager, L., Schmitt, R., Bussfeld, P., Pogarell, O., Moller, HJ., Juckel, G., Hegerhl, U., 2004. Integration of fMRI and simultaneous EEG: towards a comprehensive understanding of localization and time-course of brain activity in target detection. NeuroImage 22, 83–94.

Mulert, C., Jager, L., Propp, S., Karch, S., Stormann, S., Pogarell, O., Moller, H.J., Juckel, G., Hegerl, U., 2005. Sound level dependence of the primary auditory cortex, simultaneous measurement with 61-channel EEG and fMRI. NeuroImage 49, 49–58.

Mukamel, R., Gelbard, H., Arieli, A., Hasson, U., Fried, I., Malach, R., 2005. Coupling between neuronal firing, field potentials, and fMRI in human auditory cortex. Science 309, 951–954.

Nagai, Y., Critchley, H.D., Featherstone, E., Fenwick, P.B., Trimble, M.R., Dolan, R.J., 2004. Brain activity relating to the contingent negative variation, an fMRI investigation. NeuroImage 21, 1232–1241.

Nebel, K., Stude, P., Wiese, H., Muller, B., de Grieff, A., Forsting, M., Diener, H.C., Kiedel, M., 2004. Sparse imaging and continuous event-related fMRI in the visual domain, a systematic comparison. Hum. Brain Mapp. 24, 130–143.

Niazy, R.K.N., Beckmann, C.F., Iannetti, G.D., Brady, J.M., Smith, S.M., 2005. Removal of fMRI-environment artefacts using optimal basis sets. NeuroImage 28 (3), 720–737.

Novitski, N., Ahlo, K., Korzyukov, P., Carlson, S., Martinkauppi, S., Escera, C., Rinne, T., Aronen, H.J., Naatanen, R., 2001. Effects of acoustic gradient noise from functional magnetic resonance imaging on auditory processing as reflected by event-related brain potentials. NeuroImage 14, 244–251.

Pantev, C., Elbert, T., Lutkenhoner, B., 1994. Oscillatory Event-Related Brain Dynamics. Plenum, New York.

Pfurtscheller, G., Neuper, Ch., Andrew, C., Edlinger, G., 1997. Foot and hand area mu rhythms. Int. J. Psychophysiology 26, 121–135.

Picton, T.W., Hillyard, S.A., Krauz, H.I., Galambos, R., 1974. Human auditory evoked potentials. I: Evaluation of components. Electroenceph. Clin. Neurophysiol. 36, 179–190.

Ritter, P., Becker, R., Graefe, C., Villringer, A., 2007. Evaluating gradient artifact correction of EEG data acquired simultaneously with fMRI. Mag. Reson. Imaging 25, 923–932.

Salek-Haddadi, A., Merschhemke, M., Lemieux, L., Fish, D.R., 2002. Simultaneous EEG-correlated ictal fMRI. NeuroImage 16, 32–40.

Salmi, J., Rinne, T., Degerman, A., Alho, K., 2007. Orienting and maintenance of spatial attention is audition and vision: an event-related brain potential study. Eur. J. Neurosci. 25 (12), 3725–3733.

Scarff, C.J., Reynolds, A., Goodyear, B.G., Ponton, C.W., Dort, J.C., Eggermont, J.J., 2004a. Simultaneous 3 T fMRI and high-density recording of human auditory evoked potentials. NeuroImage 23, 1129–1142.

Scarff, C.J., Dort, J.C., Eggermont, J.J., Goodyear, B.G., 2004b. The effect of MR scanner noise on auditory cortex activity using fMRI. Hum. Brain Mapp. 22, 341–349.

Schabus, M., Dang-Vu, T.T., Albouy, G., Balteau, E., Boly, M., Carrier, J., Darsaud, A., Degueldre, C., Desseilles, M., Gais, S., Phillips, C., Rauchs, G., Schnakers, C., Sterpenich, V., Vandewalle, G., Luxen, A., Maquet, P., 2007. Hemodynamic cerebral correlates of sleep spindles during human non-rapid eye movement sleep. Proc. Nat. Acad. Sci. U. S. A. 104 (32), 13464–13469.

Shah, N.J., Jancke, L., Grosse-Ruyeken, M.L., Muller-Gartner, H.W., 1999. Influence of acoustic masking noise in fMRI of the auditory cortex during phonetic discrimination. J. Magn. Reson. Imaging. 9, 19–25.

Speckmann, E.J., Elger, C.E., 2004. Introduction to the neurophysiological basis of the EEG and DC potentials. In: Niedermeyer, E, Lopes da Silva, F (Eds.), Electro-encephalography: Basic Principles, Clinical Applications, and Related Fields. Lippincott and Williams.

Smith, S., 2002. Fast robust automated brain extraction. Hum. Brain. Mapp. 17, 143–155.

Talavage, T.M., Edminster, W.B., 1998. Saturation and nonlinear fMRI responses in auditory cortex. NeuroImage 7, S362.

Talavage, T.M., Edminster, W.B., Ledden, P.J., Weisskoff, R.M, 1999. Quantitative assessment of auditory cortex responses induced by imager acoustic noise. Hum. Brain Mapp. 7, 79–88.

Thaerig, S., Behne, N., Schadow, J., Lenz, D., Scheich, H., Brechmann, A., Herrmann, C.S., 2007. Sound level dependance of auditory evoked potentials: simultaneous EEG recording and low-noise fMRI. Int. J. Psychophysiology. 67 (3), 235–241.

Warbrick, T., Bagshaw, A.P., 2008. Scanning strategies for simultaneous EEG–fMRI evoked potential studies at 3 T. Int J. Psychophysiol. 67 (3), 169–177.

Woolrich, M., Ripley, B., Brady, J.M., Smith, S., 2001. Temporal autocorrelation in univariate linear modelling of fMRI data. NeuroImage 14, 1370–1386.

Woolrich, M., Behrens, T., Beckmann, C., Jenkinson, M., Smith, S., 2004. Multilevel linear modeling for fMRI group analysis using Bayesian inference. NeuroImage 21, 1732–1747.

Wronka, E., Kunlecki, M., Kalser, J., Coenen, A.M., 2007. The P3 produced by auditory stimuli presented in a passive and active condition, modulation by visual stimuli. Acta Neurobiol. Exp. (Wars). 67 (2), 155–164.

Yordanova, J., Kolev, V., Heinrich, H., Woemer, W., Banaschewski, T., Rothenberger, A., 2002. Wavelet entropy analysis of event-related potentials indicates modality-independent theta dominance. Euro. J. Neurosci. 16 (11), 2214–2224.